Non-Fickian dispersivity investigation from numerical simulations of tracer transport in a model double-porosity medium at different saturations

T.D. (Tiến Dũng) Tran Ngoc[a,b,*], Azita Ahmadi[c], Henri Bertin[c]

[a] Centre Asiatique de Recherche sur l'Eau (CARE), Ho Chi Minh City University of Technology (HCMUT), 268 Ly Thuong Kiet St., Dist. 10, Ho Chi Minh City, Viet Nam
[b] Vietnam National University, Ho Chi Minh City, Viet Nam
[c] Institut de Mécanique et d'Ingénierie (I2M), UMR CNRS 5295, Université de Bordeaux, ENSAM, INP Bordeaux, 33400 Talence, France

Non-Fickian dispersivity
experiment
numerical simulation
saturation dependence
double-porosity medium

A B S T R A C T

It is generally admitted that dispersivity is an indicator of the heterogeneity scale of porous media. This parameter is assumed to be an intrinsic property which characterizes the dispersive behavior during the transport of a tracer in a porous medium. When the medium is saturated by two fluid phases (water and air), dispersivity depends strongly on saturation. "Double-porosity" medium concept can be attributed to a class of heterogeneous soils and rocks in which a strong contrast in local pore size characteristics is observed. In this work, we characterized non-Fickian dispersivities of a double-porosity medium at different saturations, by performing numerical simulations for a series of one-dimensional experiments of tracer dispersion under different initial and boundary conditions. The physical double-porosity model was composed of solidified clayey spheres, distributed periodically in a more permeable sandy matrix. Using a two-equation macroscopic model, numerical simulations reproduced very well the experimental data, thus allowing to determine the dispersivity for different transport scenarios. For the first time, the existence of a unique dispersivity of a double-porosity medium at a given saturation was demonstrated for different transport scenarios of initial and boundary conditions. The saturation dependence of the dispersivity in the double-porosity medium was established and compared with the trends obtained for the single-porosity soils in previous studies.

1. Introduction

Prediction of solute transport in a geological medium requires a thorough understanding of both physiochemical-biological processes and porous medium properties. One of the key processes is the dispersive transport mechanism that can be characterized by the dispersivity (Bear, 1972). This parameter is generally defined as the ratio between the dispersion coefficient and the flow velocity (Bear, 1972; Fetter, 1999). It is empirically determined from concentration measurements (evolution with time and space) during laboratory and field tracer tests by using conventional/advanced models of convection-dispersion or spatial moments analysis (Aris, 1956; Fried, 1975; Gaudet et al., 1977; Khan and Jury, 1990; Gelhar et al., 1992; Vanderborght and Vereecken, 2007; Tran Ngoc et al., 2011; Robert et al., 2016). The existence of a unique dispersivity within an infinite heterogeneous medium was regarded in theoretical investigations of the scale effect on dispersivity (Gelhar et al., 1979; Matheron and De Marsily, 1980). Although it is largely admitted that dispersivity is an intrinsic soil property, rare studies, especially for heterogeneous media, have shown a unique dispersivity as an intrinsic value which could be simultaneously used to reproduce different breakthrough curves (BTC) under different transport boundary conditions.

Solute transport observed in porous heterogeneous media is often non-Fickian, i.e. preferential transport, earlier arrival and tailing effect in BTCs, due to scale-dependent dispersion/dispersivity (Wheatcraft and Tyler, 1988; Sternberg et al., 1996). A general consensus about the scale-dependent dispersivity has been reported by many laboratory and field researches over the last few decades (Silliman and Simpson, 1987; Gelhar et al., 1992; Irwin et al., 1996; Pachepsky et al., 2003; Huang et al., 2006, among others). It means that during solute transport in heterogeneous media the dispersivity increases with travel distance (thus with time) in a pre-asymptotic stage before reaching a constant value (Gelhar, 1987; Mishra and Parker, 1990; Suresh Kumar et al., 2006; Sharma and Abgaze, 2015). Irwin et al. (1996) showed that dispersion may be dependent upon the scale of a characteristic length (travel distance) from their KCl tracer transport experiment in a medium with periodic heterogeneity. However, the experiments of Sternberg et al. (1996) pointed out that dispersion coefficient could

* Corresponding author.
E-mail address: tntdung@hcmut.edu.vn (T.D.T.D. Tran Ngoc).

https://doi.org/10.1016/j.jconhyd.2020.103678

increase or decrease depending on the heterogeneity arrangement of glass particle sets in periodic heterogeneous porous media. Majdalani et al. (2015) conducted several replicable transport experiments in a periodic heterogeneous medium, composed of a set of PVC columns containing glass spheres surrounding a cylindrical cavity placed in the center of the column, acting as a wide pore that induces preferential water and solute transfer. They found statistically that the dispersion coefficient could be a function of the medium length or not, taking into account sampling effects. Recently, from small- and large-scale experiments with different soil volumes (0.15 – 0.60 m in column length and 0.1 – 0.2 m in diameter) performed in tropical intact soil columns, Godoy et al. (2018) pointed out an increasing trend of the dispersivity with column lengths fitted by exponential functions due to heterogeneous arrangements in soil samples, but no clear dependence of the dispersivity on sample diameters and volumes was observed.

In the meanwhile, there has been no general conclusion concerning the saturation-dependent dispersivity for unsaturated media. A correlation between the increase of dispersivity with decreasing saturation has been stated according to the investigation of tracer dispersion experiments in homogeneous sand columns (single-porosity media) (Yule and Gardner, 1978; De Smedt et al., 1986; Haga et al., 1999; Padilla et al., 1999; Nützmann et al., 2002; Latrille, 2013). However, Raoof and Hassanizadeh (2013) proposed a non-monotonic relation of the dispersivity with saturation. This relation is compatible with the results of hydrodynamic dispersion experiments of Toride et al. (2003) in unconsolidated sand columns under variably saturated conditions. They observed for intermediate values of water saturation, an increase of the dispersivity as the saturation decreases, while the contrary is reported for small saturations. The experimental results of other authors (Maraqa et al., 1997; Sato et al., 2003; De Witte, 2017) showed also a non-monotonic variation of the dispersivity as a function of the saturation (see in Tran Ngoc et al., 2017). It should be noted that saturation distribution profiles were directly measured in a few studies (Toride et al., 2003; Latrille, 2013). It is also worthwhile to note that non-Fickian transport was observed in homogeneous unsaturated media (single-porosity media) for saturation profiles, stated uniform throughout the columns, established by unit gravitational hydraulic gradient (Yule and Gardner, 1978; Maraqa et al., 1997; Toride et al., 2003), but mostly Fickian transport for uniform saturation profiles were established by controlled air suction (Sato et al., 2003). Using a porous micro-model made of a polymer for the dispersion experiments of an ink-water system, Karadimitriou et al. (2016, 2017) confirmed a parabolic behavior of dispersion coefficients with saturations (leading to non-monotonic dispersivities) because of the absence (high saturation) or presence (small saturation) of stagnant zones in the porous medium. Juarez-Morejon (2017) found an increase of the dispersivity with smaller saturations in a series of experiments simulating crude oil recovery by flooding of water and polymer solution in a homogeneous sandstone. Therefore, the practice of performing numerical simulations for real-life transport problems using as the dispersivity value an estimate based on the length of the contaminant plume or the distance between the source and specific measurement points (travel distance) (Sudicky, 1986; Freyberg, 1986), has to be considered with caution. Moreover, this practice would not lead to a good estimate without taking into account the dependency of dispersivity upon saturation, especially for transport problems in a heterogeneous vadose zone.

Dispersivity studies for unsaturated heterogeneous media are less numerous compared to those for homogeneous media. Indeed, laboratory experiments conducted to investigate saturation-dependency of the dispersivity in unsaturated heterogeneous media are scarce in the literature. A class of heterogeneous media can be studied by the concept of “double-porosity” media (Barenblatt et al., 1960) in which a contrast in local macro-micro pore size characteristics is observed. Solute dispersion phenomena in the macro-pores with interactions/exchanges with micro-pores are commonly observed (Gerke and van Genuchten, 1993; Schwartz et al., 2000; Singha, 2017, among others). This leads to non-Fickian behavior characterized by a corresponding dispersivity. The available dispersivity-saturation relationship for single-porosity media may be applicable for double-porosity media if the convective flux and thus dispersion only takes place only in the mobile zone represented by the macro-pore domain. However, a study on the relation between the non-Fickian dispersivity and water saturation for transport in a double-porosity medium is still needed to provide a confirmative proof, because dispersion also depends on heterogeneity of microstructure in such media as well as dispersion in the macro-pore domain and diffusion in the micro-pore domain. To our knowledge, no trend has been established for this relation in a double-porosity medium with a known microstructure. Golfier et al. (2011) used experiments of solute transport in a bimodal medium (fine sand inclusions surrounded by coarse sand) to study the impact of injection conditions on the Fickian or non-Fickian transport, using the same dispersivities for the two material constituents in numerical simulations by macro-scale models. Under saturated conditions, Paterson et al. (1996) found a dispersivity of 0.04 cm at the transition regime of diffusion-dispersion (Péclet number ~ 1) for a double-porosity medium made of porous grains with the permeability ratio between intra- and extra-grain domain of 2.5×10^{-2}. This dispersivity value is of the same order of magnitude as the heterogeneity size (mean grain diameter of 0.05 cm). Tran Ngoc et al. (2007) carried out tracer dispersion experiments in an unsaturated periodic double-porosity medium to validate a theoretical macroscopic model of the two-equation type (Tran Ngoc et al., 2011) and to highlight qualitatively double-porosity effects in non-Fickian behaviors (Tran Ngoc et al., 2014). The double-porosity medium is a physical model column at which the REV (Representative Elementary Volume), equivalent to a period, is well controlled by the microstructure of two constituents of strong hydraulic contrast (sintered clay spheres and sand). In a similar periodic double-porosity medium, a KBr transport experiment was done under unsaturated conditions by water infiltration and suction applied at the column inlet and outlet, respectively (Peng et al., 2015). For this heterogeneous medium, a dispersivity value of 0.13 cm was fitted for the obtained breakthrough curve which is smaller than the diameter of the clayey spheres (heterogeneity of medium) of 0.5 cm, although of the same order of magnitude.

Non-Fickian transport appearing in BTC data may possibly be a result of different superimposed physical, chemical and biological effects. In this work, our focus will be on anomalous dispersion due to physical effects and more particularly to the microstructure of the porous medium under study. Thus, it is necessary to carry out tracer transport experiments in a physical double-porosity medium with controlled microstructure under various physical frameworks: different saturation profiles and different exterior loadings. A BTC database constituted from these experiments will allow one to provide a proof of the existence of a dispersivity value that enables characterization of the non-Fickian BTCs for different transport scenarios.

The main objective of this study is to investigate the non-Fickian dispersivity of a double-porosity medium, the dependence of this parameter on the saturation in double-porosity medium and to compare the trends obtained with those observed for the single-porosity media in previous studies. To this end, we analyze the dataset of the experiments presented in Tran Ngoc et al. (2011, 2014) and of a new series of one-dimensional dispersion experiments performed under different initial and boundary conditions. The experimental BTC are fitted with those obtained by numerical simulations using the conventional and upscaled convection-dispersion model in order to identify dispersivity values for single- and double-porosity media with different saturations, respectively. A description of the experiment and new data analysis methods are presented in the two next sections. After that, the results and discussions are presented. The conclusions of the study will be addressed in the final section.

2. Materials and experimental methods

2.1. One-dimensional physical model of double-porosity medium

The physical model of the double-porosity medium used in this study was initiated by Lewandowska (2004). It was constructed from fine sand Hostun HN38 and clay spheres which were washed and hand-modeled in a spherical form with an average radius R of 0.32 cm and then fired at 1000°C in a pottery furnace. These two geo-material constituents come from the aquifers of Hostun (Southeastern France) and La Bisbal (Northeastern Spain), respectively. The mineralogic analysis by X-Ray diffraction indicated Si and Si/Al/Ca/Fe for the main chemical composition of the sand and clay (montmorillonite type), respectively (Tran Ngoc, 2008). The physical and hydrodynamic properties of two porous media were investigated by Lewandowska et al. (2005, 2008); Tran Ngoc et al. (2011, 2014) and thus are reported in Table 1.

The formation of the double-porosity physical medium follows the same principle as that presented in previous studies (Lewandowska et al., 2005, 2008; Szymkiewicz et al., 2008; Tran Ngoc, 2008; Tran Ngoc et al., 2011; Lewandowska and Pilawski, 2012; Tran Ngoc et al., 2014). The HN38 sand and solidified clay spheres play the role of the macro-pores (between the sand grains) and micro-pores (inside the spheres) in the double-porosity medium, respectively. They were interlayered in a manner keeping a volumetric fraction (ratio between the volume of each material constituent including solids and pores and the total volume of the sample) of about 50% for each porous material. We filled up about 65 layers of each constituent in an acrylic circular column of 6 cm inner diameter to reach the heights of about 50 cm (Table 2). Note that the first and last layers in the columns were composed of the sandy matrix to envelop clay spheres. In this way, a column of the pseudo-periodic double-porosity medium is constructed (Fig. 1a and b) with a 3D periodic microstructure of $0.64 \times 0.64 \times 1.3$ cm^3 modelled by the scheme of Fig. 1c. This periodic cell is the REV of the medium. The hydraulic conductivity at 100% saturation (by pure water) of the obtained double-porosity medium was expected to be slightly smaller than 1.50×10^{-3} cm/s determined by brine injection (Tran Ngoc, 2008), due to the viscosity difference between water and brine. The hydraulic conductivity of 0.97×10^{-3} cm/s at very close to saturation (about 85%) was determined by using an infiltrometer (Jougnot, 2006; Jougnot et al., 2008). The double-porosity medium here is heterogeneous on the scale of observation but could be considered as a homogeneous medium on the scale of measurement. This may be consistent with natural soils, even if our physical model could not represent natural porous formations (Sternberg et al., 1996).

We also built single-porosity medium columns by filling up only Hostun 38 sand in the same columns used for the double-porosity medium model. The sand was compacted in a controllable manner to obtain the same porosity as the one measured for the sand matrix in the double-porosity medium (Table 2).

Table 1
Main soil properties of two geo-material constituents used for creating the model double-porosity medium.

Property		Sand	Clay
Grain density, ρ_g	[g/cm^3]	2.65	2.91[a]
Dry bulk density, ρ_d	[g/cm^3]	1.59	1.89[a]
Average grain diameter, d_{50}	[μm]	162	–
Pore-size, Ξ	[μm]	10 – 500[c]	0.1 – 1[a]
Porosity, n	[–]	0.400	0.348[a]; 0.343[b]
Hydraulic conductivity, K_S	[cm/s]	2.87×10^{-3}	1.96×10^{-6}
Air entry pressure, h_a	[cm of H_20]	90	165

[a] Average values obtained by two different mercury injection tests for two different clay spheres.
[b] By gamma ray measurement for a cylindrical sample (25.9 cm high and 5.25 cm diameter) made of the same clay as the solidified clay spheres; [c] Vitorge et al., 2013).

2.2. Dispersion experiments

The experimental setup used for the different stages of the dispersion experiments (Fig. 2) in the double-porosity medium is presented in Tran Ngoc et al. (2011, 2014). The first stage concerns the establishment of saturated/unsaturated steady-state flow using a volumetric pump (Amersham Biosciences Pump P-500) for imposed inflow rate control and a balance linked to a data logger (Campbell Scientific Ltd CR 10X) for outflow rate control. The dispersion tests were only launched when an identical flow rate is obtained for both inflow and outflow. The inlet flux (Darcy velocity) was imposed from the bottom (except for Test 4) by using the volumetric pump to limit possible density-driven effect. For Test 4, the inlet flow was supplied by the pump from the top with an applied suction of $h = -85$ cm of H_2O at the column bottom. This suction application induced an average water content of 0.298 for the entire medium (Fig. 3a). The soil columns were placed in the gamma ray mobile rig to measure locally the water contents inside the column (from which the saturation degree is deduced) before performing the dispersion stage (Gharbi et al., 2004). The gamma ray device consists of a radioactive ^{241}Am source, a scintillator and a photomultiplicator allowing to determine the water content with a precision of 3%.

To obtain fully saturated samples for dispersion experiments (Tests 1 and 8), the initially dry soil columns were saturated by carbon dioxide gas before establishing the flow. For other tests under unsaturated conditions, the CO_2 was not injected into initially dry soil columns. The influx was entered from the column base without maintaining a low pressure at the outlet (Tests 2, 3, 5, 6 and 7 for the double-porosity columns and Tests 9 and 10 for the single-porosity columns). So, the particular unsaturated condition was attained due to air trapping in the medium (water content inside the medium is smaller than total porosity). Dead-end pores may only exist in the micro-porosity or immobile water domain (clay spheres), but this is an acceptable assumption for the dispersion in mobile-immobile systems when we consider no flow in this domain. The measured water content in this unsaturated condition can be considered as the effective porosity for the forthcoming dispersion experiments. Using the gamma attenuation technique, the saturated/unsaturated conditions were confirmed by comparison between water contents θ and total porosities (equal to saturated water content θ_S) (Fig. 3).

The water content profiles measured inside the single- and double-porosity medium columns provided a clear indication on the unsaturated conditions for dispersion experiments, i.e. when $\theta < \theta_S$, Fig. 3. Here θ can be considered as the effective porosity and θ_S as the total porosity. Note that the measured average θ_S (0.3988) is in perfect agreement with the total porosity determined by weighting (0.3989) for Test 8 (single-porosity medium), while a difference of 3% for Test 1 (double-porosity medium) between the measured average θ_S (0.353) and the total porosity (0.364) calculated by $n_1 \times w_1 + n_2 \times w_2$ (see Table 2 for annotations of n_1, n_2, w_1 and w_2). Note also that the measured values of water contents in the vicinity of the top and bottom of the samples were biased due to diffracted gamma ray attenuation in these zones (Fig. 3). The distribution of the water contents is highly influenced by the presence of heterogeneity in the medium (i.e. clay spheres) (Fig. 3b), while it remains fairly uniform for single-porosity medium columns (Fig. 3a). It must be noted that in spite of using gamma ray attenuation technique, it is still very difficult to figure out the water re-distribution induced by the heterogeneities. For the double-porosity medium columns, the water content profiles are available only for Tests 1, 2 and 4.

The NaCl tracer dispersion was launched in the final stage by switching water to tracer solution or vice-versa, according to the

Table 2
Characteristics and conditions of the dispersion experiments.

Test	Column	Type	L	n_1	n_2	w_1	w_2	m_1	m_2	S_w	T_{avg}	q	C_{ini} [g/l]		C_{inj} [g/l]	
			[cm]	[-]	[-]	[-]	[-]	[g]	[g]	[%]	[^{0}C]	[cm/s]	C'_{ini}	C''_{ini}	C'_{inj}	C''_{inj}
1	A	Step	50.4	0.389	0.343	0.484	0.516	1117	1379	100	19.3	5.90E-04	20	0.90	0	0.90
2	B	Step	51.0	0.378	0.343	0.490	0.510	1168	1381	86	20.7	3.44E-04	0	0.90	5	0.90
3	C	Step	46.9	0.386	0.343	0.483	0.517	1044	1289	*	20.3	3.44E-04	0	0.90	5	0.90
4	B	Step	51.0	0.378	0.343	0.490	0.510	1168	1381	82	20.1	3.44E-04	0	0.70	5	0.70
5	B	Pulse	51.0	0.378	0.343	0.490	0.510	1168	1381	*	24.4	3.44E-04	0	1.27	5	1.04
6	C	Pulse	46.9	0.386	0.343	0.483	0.517	1044	1289	*	20.5	3.44E-04	0	0.95	5	0.95
7	C	Step	46.9	0.386	0.343	0.483	0.517	1044	1289	*	19.9	5.90E-04	5	0.90	0	1.10
8	D	Step	50.1	0.399				2413		100	19.1	5.90E-04	20	0.40	0	0.40
9	E	Step	50.3	0.404				2434		86	21.2	3.44E-04	0	0.40	5	0.40
10	F	Step	50.2	0.400				2440		87	22.2	3.44E-04	0	0.40	5	0.40

(Tests 1 – 7 stand for the double-porosity medium (combination of sand and clay spheres) and Tests 8 – 10 for the single-porosity medium (pure sand). L is the length of the medium column; w_1 and w_2 are the volumetric fractions of the sand (macro- porosity domain) and of the clay (micro-porosity domain), respectively; m_1 and m_2 are the masses of the sand and clay spheres, respectively; $S_w = <\theta> / <n>$ is the average saturation degree, n_1 and n_2 are the porosities of the sand and clay spheres; T_{avg} is the average temperature; q is the imposed water flux (Darcy velocity); $C_{ini} = C'_{ini} + C''_{ini}$ is the initial concentration where C'_{ini} is the intentionally imposed salt concentration and C''_{ini} is the estimated concentration of minerals in the solution of medium; $C_{inj} = C'_{inj} + C''_{inj}$ is the applied concentration where C'_{inj} is the intentionally imposed salt concentration and C''_{inj} is the estimated concentration of minerals in the influent solution. For the tests of pulsewise type, the pulse duration is of $t_0 = 4620$ s with a pulse concentration $C_p = 5$ g/l. * not available but the S_w of 86% of Test 2 can be assumed for Tests 3, 5, 6 and 7).

selected boundary and initial conditions (water displaced or displacing tracer solution) (Fig. 2). In almost all dispersion tests (except Tests 1, 7 and 8), the higher concentration solution was used as displacing solution, while the smaller concentration solution was chosen as the displaced solution to avoid viscous fingering since at room temperature viscosity is lower for more concentrated solutions (Table 2). Two boundary conditions were used in this study: i) stepwise-like condition where an imposed salt concentration in the influent solution was continuously injected at the column inlet and ii) pulsewise-like condition where a concentration pulse was injected within a given duration at the column inlet. The later condition was obtained by using a four-line valve in order to switch the water pump into the NaCl solution pump (starting to inject the imposed concentration) and vice-versa (ending concentration pulse). After the tracer dispersion process, the column was moved to the gamma ray device to measure once again the water content. The water used in the experiments was purified by a reverse osmosis apparatus (Milli-ro 3 Plus) but some minerals possibly remained. The evolution of tracer concentration with time (breakthrough curves – BTC) was monitored by measuring the density of the effluents every 150 – 300 s by a densitometer (Anton Paar, mPDS 2000). During the tests, this densitometer recorded also the laboratory room temperature. The precision of the density and temperature is 0.005% and 1% of the measured values, respectively. A temperature difference of 0.1 °C might result in a density error of up to 0.0001 g/cm^3.

A series of dispersion tests were carried out in the model double-porosity medium. For the experiments under unsaturated conditions, the tests with stepwise-like and pulsewise-like brine injection were successively performed in the same double-porosity medium: Tests 2, 4 and 5 (same column B) and Tests 3, 6 and 7 (same column C) (Table 2). The NaCl concentration of the tracer solution was higher in the test under the saturated condition than in the tests under the unsaturated condition (Table 2). Considering that the high salt concentration used in the experiments might influence the dispersion behavior, especially for the experiments in the double-porosity medium, the high salt concentration (20 g/l) was used only for the two first tests (Tests 1 and 8 under saturated condition) in the beginning of our dispersion experiments campaign and was changed into low concentration (5 g/l) for other tests.

For the pulse-like tests (Tests 5 and 6), a pulse of the salt tracer solution equal to a volume of about 1/10 of the total pore volume (482 cm^3) was injected in the medium during 4620 s. The main characteristics of all the dispersion tests are reported in Table 2. Parallel to the dispersion tests in the double-porosity medium, another series of dispersion tests (Tests 8 – 10) were performed in the single-porosity medium (pure sand) as a constituent of the double-porosity medium, under the same saturation conditions as the double-porosity tests (Tran Ngoc et al., 2011, 2014). Therefore, the required properties of the sand column for later numerical simulations were independently identified.

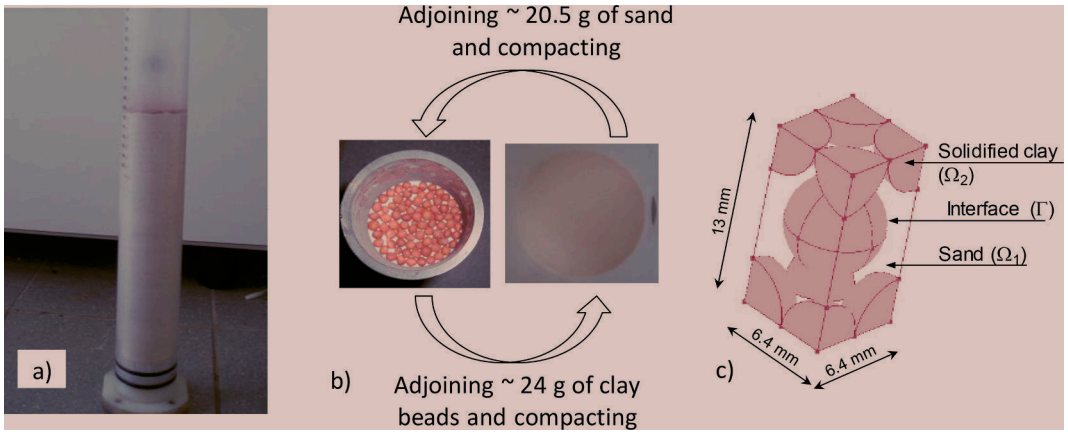

Fig. 1. Model column of the double-porosity medium being filled up periodically up to all the column (a), by interchanging the clay sphere and sand layers b, (the clay sphere layer displayed on the figure would be hidden after pouring in the column a sand layer), and c) its schematized microstructure period.

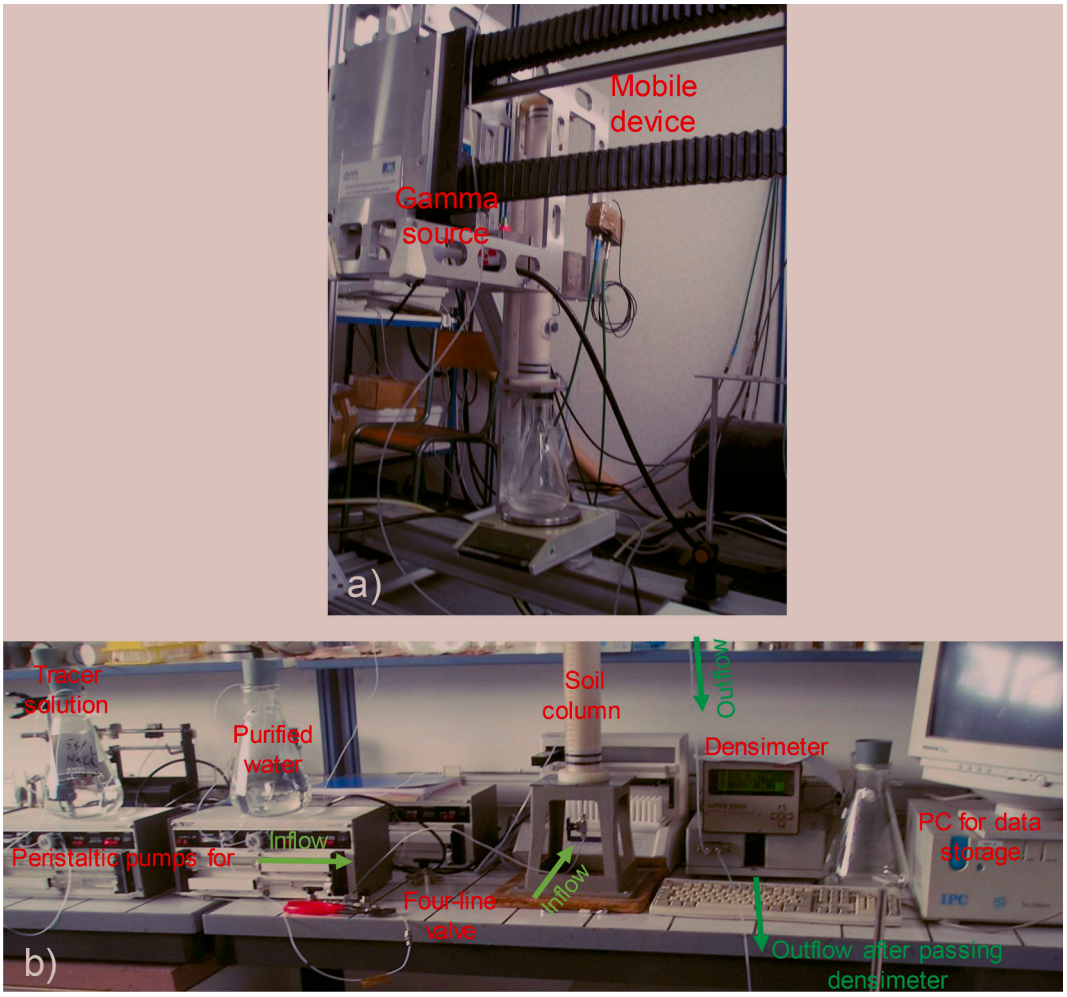

Fig. 2. Apparatus for the experiment: a) Flowing stage with water content measured by gamma ray technique; b) Dispersion stage.

The mass balance of all the tests was verified by checking the fact that the sum of the masses of salt in the influent flow, M_1, and originally in the column, M_0, is equal to the sum of the masses of salt leaving the column, M_2, and present in the column at the end of a dispersion test, M_3. To do so, we first converted the BTCs in density into BTCs in concentration using the linear relation of density – concentration at the average temperature of each test, established from International Equation of State of Seawater 1980 (Unesco-IES80) (Fofonoff and Millard Jr., 1983; Le Calvé, 2002; Millero, 2010). We were conscious that this conversion contains errors but considered it acceptable as a first estimate. The difference between the density measured by the densimeter and calculated by the IES80 is about 0.0003 g/cm^3 when fixing the concentration within the range of 1 – 6 g/l (Fig. 4). The salt mass in the effluent M_2 was then estimated at the final time of each test by using TableCurve® to calculate the area under BTC. M_0, M_1 and M_3 were calculated by taking into account mineral mass (different from salt mass imposed intentionally) that was estimated from the beginning and ending density values in the BTCs, C_{ini} and C_{inj} (Table 3). The mass error is smaller for the single-porosity columns than for the double-porosity columns. It is very small for almost all tests (< 5%), (except for Test 4 and 7 where they were 9% and 7.5% respectively) and becomes even smaller when calculated for higher of S_w. Higher saturation values were explained by the fact that the medium was saturated a little more during long lasting dispersion experiments and by the measurement precision (3%). Thus, the estimations of the concentrations C_{ini} and C_{inj} by fitting the BTCs in regarding density values at early times are acceptable. This small difference comes from the physical nature of the salt retained in the micro-pores of the clay spheres. Indeed, retained salt diffuses very slowly and therefore leads to the tailing effect of BTCs. Another reason for the difference comes from the estimations of C_{ini} and C_{inj} (see Table 2) based on the mineral mass present in the used water and released by the ion exchange of clay during the experiments and detected by the densitometer. It could also be attributed to the conversion of the measured density into concentration that was impacted by the temperature variations during dispersion tests.

3. Modelling and dispersivity determination

3.1. Governing equations

The BTCs of the brine dispersion experiments in the single-porosity medium columns (Tests 8 – 10) can be modelled by using the conventional Convection-Dispersion transport Equation (CDE), written as (Bear, 1972; van Genuchten and Wierenga, 1976; Kutílek and Nielsen, 1994):

$$\frac{\partial C}{\partial t} = D_{SP}\frac{\partial^2 C}{\partial z^2} - v\frac{\partial C}{\partial z} \quad (1)$$

where C [ML^{-3}] is the salt concentration in the flowing solution; θ [-] is volumetric water content ($S_w = 100\% \times \theta/n$, with n porosity); D_{SP} [L^{2}T^{-1}] is dispersion coefficient in the liquid phase; v [LT^{-1}] is pore velocity ($v = q/\theta$, q the imposed Darcy velocity); z [L] is the position or depth in the soil column and t [T] is the time variable. The subscript SP stands for Simple Porosity vs DP used below for Double Porosity porous

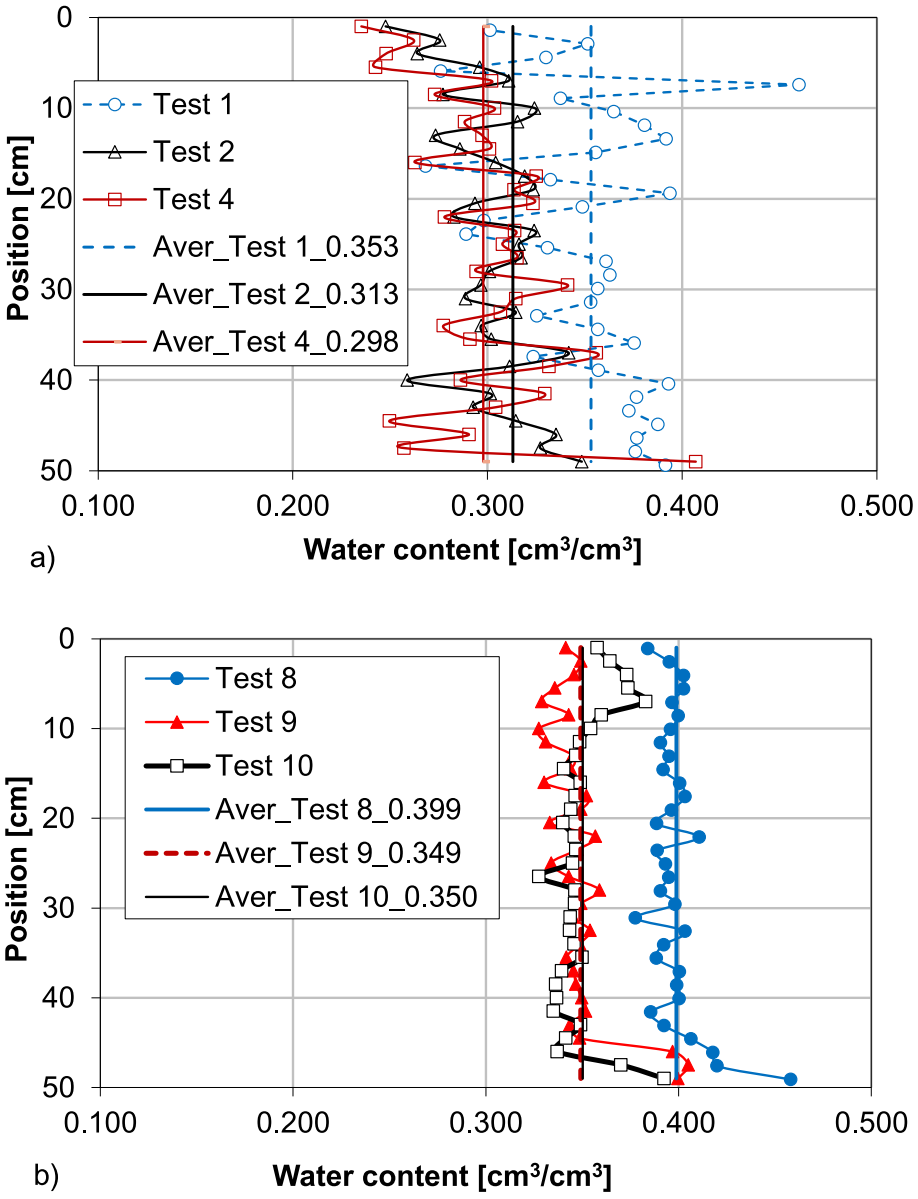

Fig. 3. Distribution of the water content inside the soil columns measured by the non-destructive technique of gamma ray attenuation after end of dispersion test. (The right lines represent for the average value of each test): a) for the double-porosity medium columns in saturated condition (Test 1) and unsaturated condition (Tests 2 and 4) and b) for the single-porosity medium columns (pure sand) in saturated condition (Test 8) and unsaturated condition (Tests 9 and 10) and (Data of these profiles were previously presented in Tran Ngoc et al., 2011, 2014).

media. The dispersivity can be written as (Bear, 1972):

$$\lambda_{SP}(S_w) = \frac{D_{SP}(S_w) - D_e}{v^{\gamma}} \tag{2}$$

In common practice for the dispersion in soils, the effective diffusion coefficient D_e [L^2T^{-1}], is considered negligible and γ is taken equal to 1, i.e. linear increase of D_{SP} with v. Thus,

$$\lambda_{SP}(S_w) = \frac{D_{SP}(S_w)}{v} \tag{3}$$

For the dispersion experiments in double-porosity medium columns, the BTCs exhibited non-Fickian features marked by an early arrival time and a tailing of salt concentration evolution. A satisfactory description of this non-standard transport could not be obtained by applying the CDE model (van Genuchten and Wierenga, 1976; Berkowitz et al., 2000; Golfier et al., 2011; Simhayov et al., 2018, among others). These BTCs can be appropriately described using two-equation models (mobile-immobile MIM) obtained from phenomenological (van Genuchten and Wierenga, 1976) or upscaling approaches (Ahmadi et al., 1998; Royer and Boutin, 2012). In these models, transport is governed by the CDE in the macro-pores and CDE or diffusion equation in the micro-pores. Here, we adopt the macroscopic dispersion – convection model obtained in Tran Ngoc et al. (2011), by applying the asymptotic homogenization technique (Auriault, 1991). This choice is motivated by the fact that this model was developed for the validation range of the experimental dispersion tests in the double- porosity medium presented above with periodic microstructure (Tran Ngoc et al., 2011) and we do not need to fit solute transfer coefficients between the macro- and micro-pores that are computed integrating all diffusive flux through surfaces of the micro-pore domain. In this model, the flow occurs only in the macro-pores (sandy matrix – domain 1 denoted Ω_1) and is stagnant in the micro-pores (clay spherical inclusions – domain 2 denoted Ω_2). This resulted from modelling water flow in an unsaturated double-porosity medium (Lewandowska et al., 2004). The

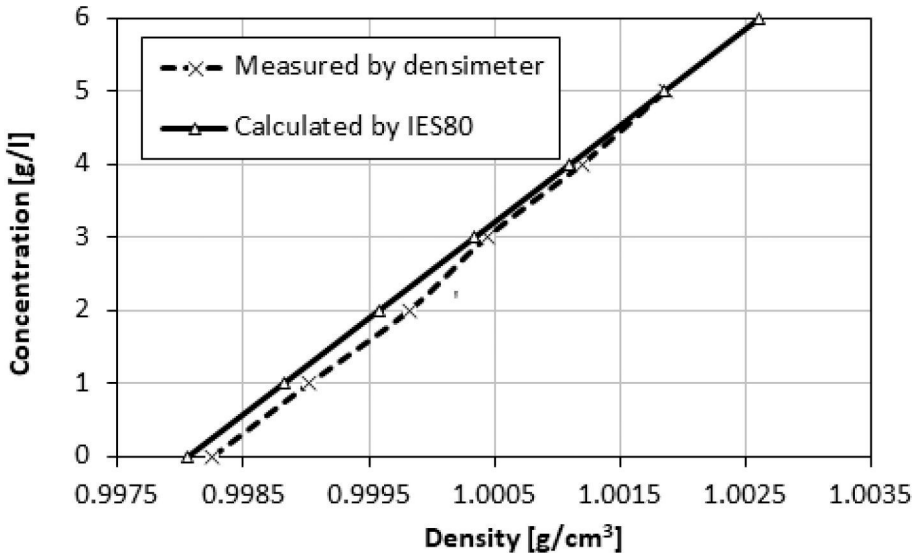

Fig. 4. Comparison of Concentration – Density between the measure and theory at the temperature of 20.7 °C.

Table 3
Salt mass balance calculated for the experiments.

Test	M_0 [g]	M_1 [g]	M_2 [g]	M_3 [g]	Mass error = $\lvert(M_0+M_1)$ - $(M_2+M_3)\rvert$ [g]	ΔM = 100% Mass error/(M_0+M_1) [%]
1	10.828	1.265	11.414	0.466	0.212	1.76
2	0.404	7.124	4.672	2.649	0.207	2.75
3	0.372	6.109	3.887	2.436	0.158	2.44
4	2.520	0.885	3.402	0.309	0.307	9.01
5	0.729	1.419	1.627	0.597	0.076	3.54
6	0.392	1.561	1.551	0.373	0.030	1.51
7	2.728	1.166	3.769	0.416	0.292	7.49
8	11.524	0.580	11.953	0.226	0.074	0.61
9	0.202	4.379	1.663	2.732	0.186	4.06
10	0.199	4.536	2.024	2.683	0.028	0.58

(Tests 1 – 7 stand for the double-porosity medium columns and Tests 8 – 10 for the single-porosity medium columns. M_1 and M_2 are the salt masses of the influent and effluent solutions; M_0 and M_3 are the salt mass present initially (before dispersion stage) and finally (end of dispersion test) in the medium. M_2 was calculated by the area below the BTC averaged from the experimental data).

transport in the domain 1 is described by the dispersion and convection mechanisms, while only diffusion is considered in the domain 2. The model is re-written for simulating the dispersion experiments mentioned above by a 1D macroscopic model coupled with a 3D problem for diffusion in the inclusions that is converted into a 1D problem in a spherical coordinate system. It is given by the following system of equations:

$$w_1\frac{\partial(\theta_1 C_1)}{\partial t} = \frac{\partial}{\partial z}\left(D_{DP}\frac{\partial}{\partial z}C_1\right) - \frac{\partial}{\partial z}(qC_1) - S \tag{4}$$

$$\frac{\partial(\theta_2 C_2)}{\partial t} = D_2\left(\frac{\partial^2 C_2}{\partial r^2} + \frac{2}{r}\frac{\partial C_2}{\partial r}\right) \text{in the domain 2} \tag{5}$$

$$C_1 = C_2 \text{ on the interface } \Gamma \text{ between the two domains} \tag{6}$$

$$S = \frac{1}{|\Omega|}\int_\Gamma \frac{\partial(\theta_2 C_2)}{\partial r}d\Gamma \tag{7}$$

where the subscripts "1" and "2" stand for the domains 1 (Ω_1) and 2 (Ω_2) respectively ($\Omega = \Omega_1 + \Omega_2$); C_1 and C_2 [ML^{-3}] are the concentration in the domain 1 and 2, respectively; w_1 [-] is the volumetric fraction of the domain 1; q [LT^{-1}] is the imposed Darcy velocity; z ($0 \le z \le L$) and r ($0 \le r \le L$) [L] are spatial coordinates; D_{DP} [L^2T^{-1}] is the dispersion coefficient of the double-porosity medium; D_2 [L^2T^{-1}] is the effective diffusion coefficient in the domain 2.

In this study the dispersivity of the double-porosity medium is defined by (Bear, 1972):

$$\lambda_{DP}(S_w) = \frac{D_{DP}(S_w)}{q} \tag{8}$$

In Eq. (8), we assumed the Darcy velocity q equal to the macroscopically averaged linear velocity relevant for the dispersion coefficient D_{DP} defined over all the porous medium in the double-porosity model (see detail in Tran Ngoc et al., 2011). Compared with the single-porosity medium (pure sand column), the dispersivity is determined by the ratio of the dispersion coefficient in liquid phase and pore velocity (Eq. 3).

The dispersion coefficients D_{SP} and D_{DP} of the dispersion tests at different water saturations were determined by fitting and validating the experimental results with numerical solutions of the above models that are presented after herein.

3.2. Numerical simulations

3.2.1. Single-porosity medium

The transport parameters of the dispersion experiments in the single-porosity medium columns, i.e. Tests 8 – 10, were found by fitting experimental BTCs with solutions of Eq. (1) using the CXTFIT code (Toride et al., 1999). To do so, the experimental BTCs in terms of density were first converted into curves in terms of relative concentration by the following relation:

$$\frac{C(t)}{C_{ini}} = \frac{\rho(t) - \rho_{min}}{\rho_{max} - \rho_{min}} \tag{9}$$

where $\rho(t)$, ρ_{min} and ρ_{max} [M/L^3] are the measured densities with time, minimal and maximal values of density in the BTCs, respectively.

Only D_{SP} was determined to avoid non-uniqueness of solution in the inverse problem, since the pore velocity v could be calculated from controlled water contents. However, various water contents were tested in the range of measured value by Gamma ray of 0.399 ± 3% × 0.399 for Test 8, 0.350 ± 3% × 0.350 and 0.350 ± 6% × 0.350 for Tests 9 and 10, due to measurement precision to get the best fit. To reproduce numerically Tests 8 – 10, D_{SP} values obtained from the above inverse problem were used in direct simulations by HYDRUS (Šimůnek et al.,

2013) with the following initial and boundary conditions:

$$0 < z < L: C(z,0) = C_{ini} \quad (10)$$

$$z = 0, t > 0: vC - D_{SP}\frac{\partial C}{\partial z} = vC_{inj} \quad (11)$$

$$z = L, t > 0: D_{SP}\frac{\partial C}{\partial z} = 0 \quad (12)$$

While the profile discretization was of 100 elements for Test 8, the profile was finely discretized into 300 elements for Tests 9 and 10 in order to avoid numerical oscillations of simulation BTC. To compare with the experimental results, the evolution of the concentration with time at the outlet element of the simulation domain was exported. The simulated BTCs in concentration were then converted into the BTCs as a function of density to be confronted directly with the measured BTCs. To this end, we used the function giving the density ρ as a function of the concentration C, the pressure P and the temperature T from the International Equation of State of Seawater 1980 (Unesco-IES80) (Fofonoff and Millard Jr., 1983; Le Calvé, 2002; Millero, 2010), taking into account the temperature data recorded simultaneously with the density in each test and the pressure value of 1.01325 MPa (equivalent to the case of standard seawater at 1 atm). The standard error related to this conversion is about 3×10^{-6} g/cm^3 (Millero, 2010). The dispersivity was determined for a saturated case (Test 8) and two unsaturated cases (Tests 9 and 10) from Eq. (3). The simulation quality indicated by statistical criteria such as the sum of squared residuals $SSQ = \Sigma(\rho_{mes} - \rho_{sim})^2$, the root mean square error $RMSE = \sqrt{\frac{\sum(\rho_{mes} - \rho_{sim})^2}{N}}$ which minimize the error and the coefficient of determination $R^2 = \frac{[\sum(\rho_{mes} - \overline{\rho_{mes}})(\rho_{sim} - \overline{\rho_{sim}})]^2}{\sum(\rho_{mes} - \overline{\rho_{mes}})^2 \sum(\rho_{sim} - \overline{\rho_{sim}})^2}$ which tends to 1, where ρ_{mes} and ρ_{sim} are the measured and simulated values of density respectively; $\overline{\rho_{mes}}$ and $\overline{\rho_{sim}}$ are the average values of measured and simulated density; and N is the number of values.

3.2.2. Double-porosity medium

The macroscopic model given by Eqs (4) – (7) was numerically implemented by using the FEM code COMSOL Multiphysics®. The implementation, detailed in Tran Ngoc et al. (2011, 2020), concerns a two-scale computation for the macroscopically 1D concentration (Eq. 4) coupled with the microscopically 1D concentration (Eq. 5, spherical transport) on the interface (Eq. 6). The coupling term is the source term in Eq. (4) which is calculated from the diffusive flux on the interface of all the microscopic domain (clay spheres) (Eq. 7) by resolving Eq. (5). To do so, a 1D geometry (L) representing the length of the double-porosity medium column in which the solute transport is described by Eq. (4), was first created (one independent variable z) in COMSOL. Then, a 2D geometry ($L \times R$) representing a series of the spheres of radius R (microscopic domain) side by side along the axis of length L was created with two independent variables z and r. Although the created geometry is 2D, the transport is considered by Eq. (5) in one-dimensional only in the R direction (radial problem) for all z positions. Through the interface (surface of the sphere), each node of the macroscopic 1D geometry is linked with a sphere in which the diffusion occurs (in the R direction). The macroscopic domain L was meshed into 100 grid blocks of the size 0.5×10^{-2} m, thus 101 nodes. After a mesh sensitivity analysis ensuring grid convergence of the results, the microscopic domain $L \times R$ was discretized very finely with 1504 grids. The meshing was regular in the z axis while it was highly refined near $r = R$ (where the coupling with the macroscopic equation is imposed) by the maximum element growth rate of 1.3 and maximum and minimum element size of 3.38×10^{-2} m and 1.51×10^{-4} m, respectively. So that, the mesh distribution consisted of two zones: a zone of 1300 quadrilateral elements (closer to the interface $r = R$ smaller elements) and another zone of 204 triangular elements (for the farthest elements from the interface). The simulation result remained unchanged for other finer meshes. To solve Eqs (4) – (7), an appropriate set of initial and boundary conditions that correspond to the experimental conditions are required. Table 4 presents the initial and boundary conditions for all the dispersion tests. Note that a third-type boundary condition was used to prescribe the concentration flux at the inlet boundary for better reproduction of the dispersion tests rather than the concentration boundary condition of the first-type (van Genuchten and Parker, 1984; Schoen et al., 1999; Cushman and Tartakovsky, 2016).

Table 4
Initial and boundary conditions for the numerical simulation of the dispersion experiments.

Type	Eq. 4		Eq. 5	
	Initial condition	Boundary condition	Initial condition	Boundary condition
Stepwise tests (1 – 4 and 7)	$C_1 = C_{ini}$	$z = 0, t > 0$: $qC_1 - D_{DP}\frac{\partial C_1}{\partial z} = qC_{inj}$ $z = L, t > 0$: $D_{DP}\frac{\partial C_1}{\partial z} = 0$	$C_2 = C_{ini}$	$r = 0, t > 0$: $D_2\frac{\partial C_2}{\partial r} = 0$ $r = R, t > 0$: $C_2 = C_1$
Pulsewise tests (5 and 6)		$z = 0, t \le t_0$: $qC_1 - D_{DP}\frac{\partial C_1}{\partial z} = qC_p$ $z = 0, t > t_0$: $qC_1 - D_{DP}\frac{\partial C_1}{\partial z} = qC_{inj}$ $z = L, t > 0$: $D_{DP}\frac{\partial C_1}{\partial z} = 0$		

(For annotation of C_{ini}, C_{inj} and C_p refer to Table 2).

The conversion of concentration in the BTCs into density versus time was integrated in the numerical simulations to allow direct comparison with the experimental BTCs which are impacted by the temperature. As for the BTCs of the single-porosity medium, this conversion was made via the Unesco-IES80.

The input data required for the numerical simulations were taken from Table 2. The diffusion coefficient in the domain 2 was considered equal to that of a saturated brick, $D_2 = 7.345 \times 10^{-7}$ cm^2/s (Ahl, 2003). The water content in the domain 2 (very low hydraulic conductivity) of the double-porosity medium was set at the value $\theta_2 = n_2 = 0.343$ for all the tests. Because no flow occurs in the domain 2 in which the water was only absorbed and retained, thus the saturated value could be reached during the long time of experiments. The "trial and error" approach was used to determine the dispersion coefficient D_{DP} of the double-porosity medium by fitting the experimental BTCs with those obtained by the double-porosity model (Eqs. 4 – 7). The corresponding dispersivity is then determined by Eq. 8. For Test 1 (saturated condition), based on the statistical indicators, i.e. SSQ, R^2 and $RMSE$, the fitted D_{DP} was chosen from different simulations made with different water contents in the domain 1, θ_1 and different dispersion coefficients D_{DP}. The initial value of D_{DP} was the dispersion coefficient found in the saturated single-porosity medium, Test 8. A series of simulations were run by coupling $\theta_1 = 0.364$; 0.385 and 0.408 (deduced from the average value measured by the Gamma ray technique $< \theta >_{mes} = 0.354$; $< \theta >_{mes} + 3\% < \theta >_{mes}$ (0.364) and $< \theta >_{mes} + 6\% < \theta >$ mes (0.374), respectively) with $D_{DP} = 2.713 \times 10^{-4}$; 1.899×10^{-4} (decreased by 30%); and 3.527×10^{-4} (increased by 30%) cm^2/s. We took the case of $\theta_1 = 0.385$ (very close to porosity value, Table 2), $\theta_2 = 0.343$, $D_{DP} = 2.713 \times 10^{-4}$ cm^2/s and $D_2 = 7.345 \times 10^{-7}$ as the base case. Knowing that the diffusion coefficient D_2 plays also a key role in the non-Fickian BTC, we made a sensitivity analysis from the base case with increasing and decreasing D_2 by the factor of 2 and 5.

For Test 2, the unsaturated condition was controlled by the macroporosity domain (Domain 1). Therefore, θ_2 and D_2 were considered the same as those of the base case in Test 1. The numerical reproduction of Test 2 was done for θ_1 in the range of water content measured in the single-porosity medium columns (Tests 9 and 10) by gamma ray

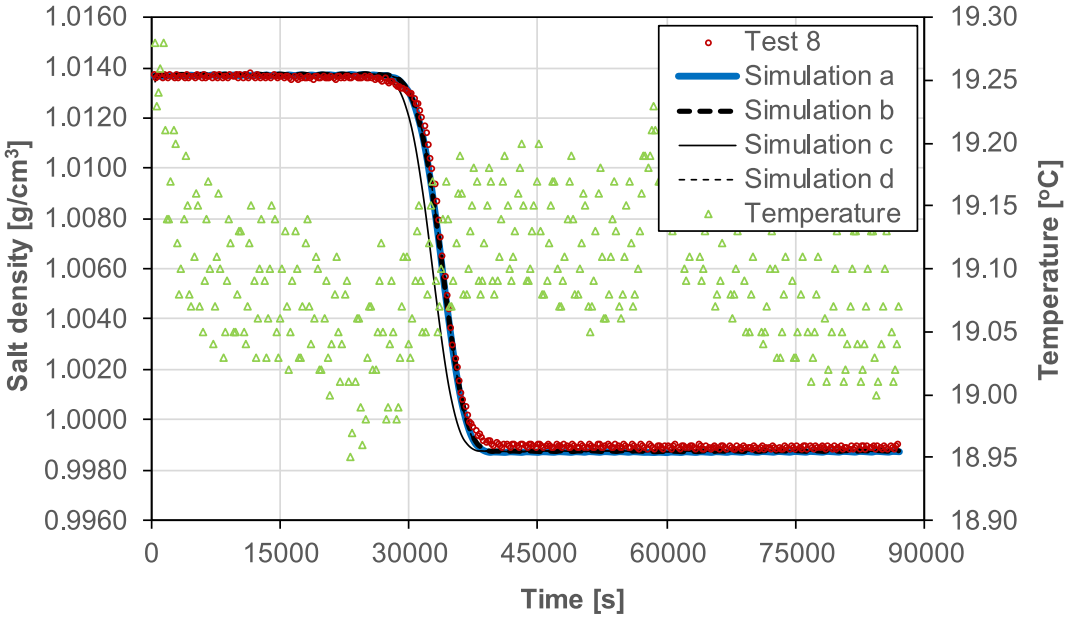

Fig. 5. Breakthrough curves obtained different simulations (see details for simulation parameters in Table 4) (lines) and the experiment (circles) with the associated temperature data (triangles) for Test 8 (single-porosity medium, saturated case). Converting the density evolution with time into the relative concentration, C/C_{ini} with pore volume exit time, V/V_p we have ratio $C/C_{ini} = 0.5$ at $V/V_p = 1$.

technique and D_{DP} in the range of dispersion coefficient fitted for the single-porosity medium columns (Tests 9 and 10) and fitted for the double-porosity medium (Test 1).

All the parameters chosen for Test 2, including the obtained dispersivity from the above fitting were used directly in the simulations for Tests 3, 5, 6 and 7. These simulations can be referred to as the validating stage for the obtained dispersivity values. For Test 4, $\theta_1 = 0.249$ was deduced from the average value of the measured water content profile (Fig. 3a) by $< \theta > = \theta_1 \times w_1 + \theta_2 \times w_2$. The fitting was done by "trial and error" to determine D_{DP} for Test 4 by starting with the dispersion coefficient of Test 2.

4. Results and discussion

4.1. Saturated and unsaturated dispersivity in the single-porosity medium

The saturated dispersivity for the single-porosity sample in Test 8 is 0.089 cm as the best fit from *Simulation d* (Fig. 5; Table 5) with $\theta = 0.401$ = porosity determined by gravity, which is very close to measured value by Gamma ray (Fig. 3b). The corresponding column Péclet number is $Pe = 1.5$ (Table 5). This dispersivity is in the order of 0.01 – 0.1 cm found for saturated unconsolidated materials in the literature (Padilla et al., 1999; Nützmann et al., 2002; Toride et al., 2003; Torkzaban et al., 2006).

As known the temperature variation influences strongly the density of the outlet solution. However, it is difficult to separate its influence due to transport mechanisms during the evolution of BTCs, especially at low temperature variation such as in Test 8 (Fig. 5). Normally, we can only observe that an increase of the temperature leads to the diminution of the density for a stage of transport, earlier times at which the concentration does not break through yet, for example (Fig. 6). In this work, the integration of the temperature in conversing of the BTCs in concentration into BTCs in density helps to minimize the influence of its variation for fitting the dispersion coefficients.

It should be noted that the BTCs in the single-porosity medium correspond to the Fickian transport, i.e. fairly symmetrical BTCs not only in the saturated case (Test 8, Fig. 5), but also in the unsaturated case (Tests 9 and 10, Fig. 6), thanks to their uniform saturation profiles (Fig. 3b). This was observed in Sato et al. (2003) for transport in uniformly unsaturated single-porosity medium columns. However, the non-Fickian transport has been often observed for unsaturated homogeneous soils (Padilla et al., 1999; Nutzmann et al., 2002; Toride et al., 2003; Bromly and Hinz, 2004). The best fit of the unsaturated dispersivity is 0.044 cm (Test 9) and 0.041 cm (Test 10) with

Table 5
Fitting parameters and errors for different simulations of dispersion tests in the single-porosity medium. (The simulation case leading to the best fit was put in italic)

Experiment	Simulation	θ	q [cm/s]	v [cm/s]	D_{SP} [cm²/s]	λ [cm]	R^2	*SSQ*	*RMSE*
Test 8	a	0.399	5.90E-04	1.48E-03	1.360E-04	0.092	0.99922	2.254E-05	2.495E-04
	b	0.411	5.90E-04	1.44E-03	1.410E-04	0.098	0.99917	2.317E-05	2.530E-04
	c	0.387	5.90E-04	1.52E-03	1.500E-04	0.098	0.98650	2.739E-04	8.699E-04
	d	*0.401*	*5.90E-04*	*1.47E-03*	*1.310E-04*	*0.089*	*0.99925*	*2.227E-05*	*2.481E-04*
Test 9	a	0.349	3.44E-04	9.85E-04	7.710E-05	0.078	0.93334	6.088E-05	4.679E-04
	b	0.360	3.44E-04	9.56E-04	3.550E-05	0.037	0.96915	2.864E-05	3.210E-04
	c	0.339	3.44E-04	1.02E-03	1.910E-04	0.188	0.88832	1.063E-04	6.182E-04
	d	*0.370*	*3.44E-04*	*9.30E-04*	*4.044E-05*	*0.044*	*0.99049*	*9.377E-06*	*1.361E-04*
Test 10	a	0.350	3.44E-04	9.82E-04	5.890E-05	0.060	0.949225	4.250E-05	1.361E-04
	b	0.361	3.44E-04	9.53E-04	3.920E-05	0.041	0.987510	1.076E-05	3.953E-04
	c	0.340	3.44E-04	1.01E-03	1.860E-04	0.184	0.909419	7.610E-05	1.989E-04
	d	*0.368*	*3.44E-04*	*9.35E-04*	*3.839E-05*	*0.041*	*0.995449*	*5.148E-06*	*1.055E-04*

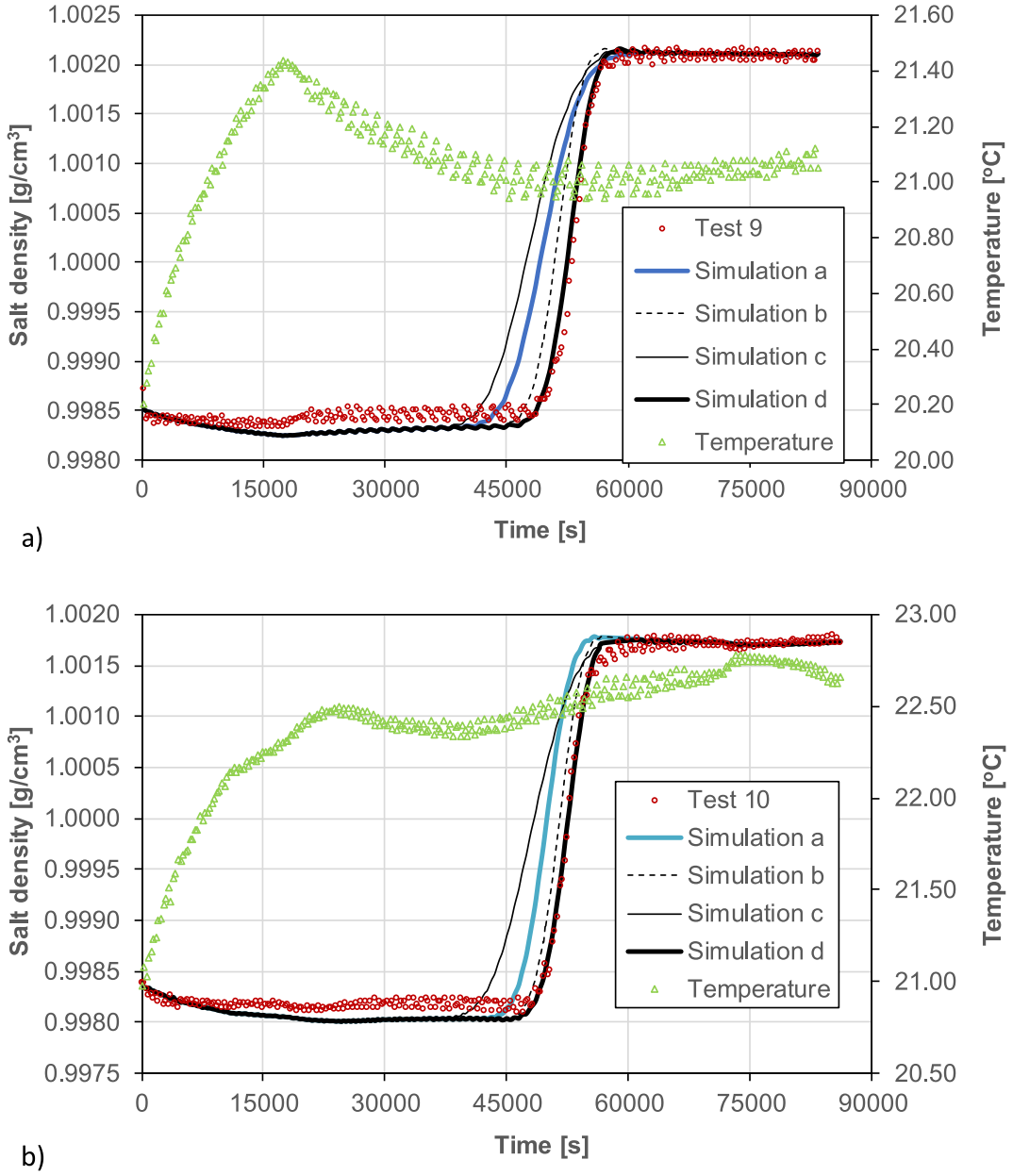

Fig. 6. Breakthrough curves obtained different simulations (see details for simulation parameters in Table5) (lines) and the experiment (circles) with the associated temperature data (triangles) for Tests 9 (a) and 10 (b) (single-porosity medium, unsaturated case). Converting the density evolution with time into the relative concentration, C/C_{ini} with pore volume exit time, V/V_p we have ratio $C/C_{ini} = 0.5$ at $V/V_p = 0.89$.

corresponding $\theta = 0.370$ and $\theta = 0.368$ (*Simulation d*, Fig. 6a and b, Table 5). The fitted water contents are greater than the measured ones by 6% for Test 9 and by 5% for Test 10 (Fig. 3b). It can be observed that the saturated dispersivity (Test 8) is greater than the unsaturated dispersivity (Test 9 and 10). However, some works in the literature showed an increase of dispersivity with a decrease of saturation (Padilla et., 1999; Nutzmann et al., 2002; Sato et al., 2003). This contradiction cannot be definitively confirmed due to the lack of other experiments with low saturation profiles. Moreover, it must be underlined that the saturated and unsaturated uniform flow condition in this study occurred for particular values of the total porosity ($\theta = 0.399$) and the effective porosity ($\theta = 0.350$) respectively (Fig. 3b). From our results, it can be concluded that the dispersivity is greater when transport takes place in the total porosity of a single-porosity porous medium than when it takes place in a part of the porosity i.e. the effective porosity.

4.2. *Saturated dispersivity in the double-porosity medium*

Both the experimental BTCs in terms of density and the temperature as a function of time are presented in Fig. 7 for three different simulations of Test 1 which corresponds to the saturated case. The simulation parameters of the best fits are reported in Table 6. It must be noted that the clay spheres where sintered at a very high temperature (1000°C) to make them resistant to aggregate dispersion and breakdown even for rather high NaCl concentrations (20 g/l). Also, compared to other tests (Tests 2 – 7) with a lower NaCl concentration (5 g/l), no particular dispersion behavior was detected in the BTC of Test 1. However, there is a slight discrepancy for the period of time $t = 0 –$ 15000 s with 0.5 °C of temperature variation, in spite of taking into account the correction of the density by temperature. In fact, the density for the period $t = 0 – 15000$ s could have been impacted not only by the room temperature, but also by other factors such as ion exchange

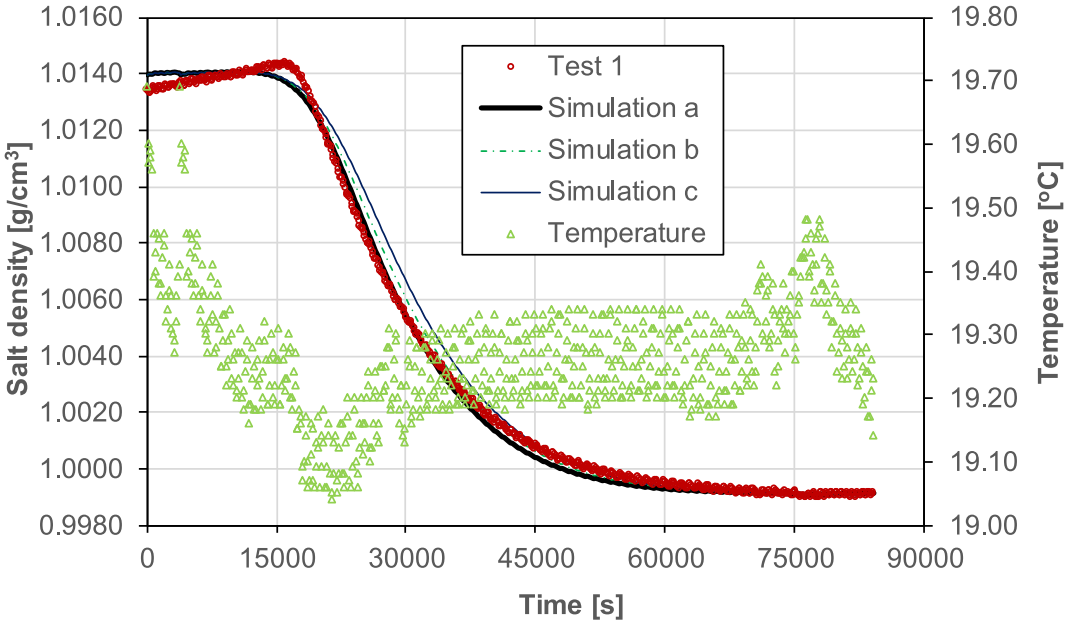

Fig. 7. Breakthrough curves obtained from different simulations (see details for simulation parameters in Table 6) (lines) and the experiment (circles) with the associated temperature data (triangles) for Test 1 (double-porosity medium, saturated case).

of clayey spheres (Dupuy et al., 2018) and/or the existence of minerals in the displacing solution (water). The effects of these factors are superimposed during the solute transport, so that it is very difficult to obtain a better fit than the one presented in Fig. 7. It should be noted that the "best" fits chosen in this study ensured to cover the non-Fickian features of experimental BTCs.

In this case, the dispersion coefficient is equal to 1.899×10^{-4} cm^2/s chosen by fitting the experimental BTC (*Simulation a*). The quality of this fitting can be evaluated by the criteria reported in Table 4. For the same Darcy velocity imposed, the obtained D_{DP} of Test 1 is greater than the D_{SP} of Test 8. Regarding the Péclet number of 4.03 (of the order of 1) for Test 1 calculated using the period size, the Darcy velocity and the dispersion coefficient and $Pe = 1.54$ for Test 8, the linear relation between the dispersion coefficient and Péclet number is respected (Fetter, 1999). Thus, the saturated dispersivity of 0.322 cm obtained is of the same order of magnitude as the heterogeneity size in the double-porosity medium, i.e. the diameter of the clay spheres of 0.64 cm. It is greater than the dispersivity (0.089 cm) found for the saturated single-porosity medium (Test 8, pure sand, one of two constituents of the double-porosity medium). The heterogeneity (clay spheres) presence in the double-porosity medium is responsible for the increase of the dispersivity (Silliman and Simpson, 1987). So far, it can be clearly seen that the dispersivity of the single-porosity medium cannot be used as the dispersivity of the double-porosity medium in spite of having the same macro-porosity.

The fitting of the BTC for the double-porosity medium columns involves two transport properties D_{DP} and D_2, which may lead to non-uniqueness of the set of coefficients determined. Therefore, only D_{DP} was fitted in this study, thus fixing D_2. Based on the base case, a sensitivity analysis to the variation of D_2 within the possible range of $1 \times 10^{-7} - 1 \times 10^{-6}$ cm^2/s for solidified clay (Jougnot et al., 2009) was conducted by performing different simulations (*d* – *g*), Fig. 8 and Table 6. Comparing BTCs for different D_2, the value of 7.345×10^{-7} cm^2/s corresponds to the best fit between the simulation and the experiment (Fig. 7). Note that the simulation only enables to reproduce the non-Fickian feature of experimental BTC if D_{DP} and D_2 is enough contrasted (*Simulation h*).

4.3. Unsaturated dispersivity in the double-porosity medium

For the unsaturated case, the simulations results fitted the experimental ones in a satisfactory manner using $\theta_1 = 0.350$. This value of the water content leads to S_w of about 90%, slightly greater than the measured value of $S_w = 86\%$ and consistent with the mass balance. For Test 2, at the early times of the BTC, the simulation respecting the principle of the density increase with decrease of temperature could not reproduced correctly the experiment at which a high density with a temperature drop was observed (Fig. 9). Together with other reasons aforementioned, this can be explainable by the fact of not complete solute washing before the dispersion test. The initial concentration was

Table 6
Fitting parameters and errors for different simulations of dispersion tests in the double-porosity medium. (The simulation case leading to the best fit was put in italic)

Experiment	Simulation	$< \theta >$	θ_1	D_2 [cm^2/s]	D_{DP} [cm^2/s]	λ [cm]	R^2	*SSQ*	*RMSE*
Test 1	*a*	*0.353*	*0.364*	*7.345E-07*	*1.899E-04*	*0.322*	*0.99821*	*5.634E-05*	*2.831E-04*
	b	0.364	0.385	7.345E-07	2.713E-04	0.460	0.99729	8.173E-05	3.440E-04
	c	0.374	0.408	7.345E-07	3.527E-04	0.598	0.99417	2.070E-04	5.426E-04
	d	0.364	0.385	1.469E-07	2.713E-04	0.460	0.95640	1.302E-03	1.361E-03
	e	0.364	0.385	3.673E-06	2.713E-04	0.460	0.97269	1.016E-03	1.202E-03
	f	0.364	0.385	3.673E-07	2.713E-04	0.460	0.99513	1.615E-04	4.793E-04
	g	0.364	0.385	1.469E-06	2.713E-04	0.460	0.98791	4.285E-04	7.807E-04
	h	0.364	0.385	7.345E-06	2.713E-03	4.598	0.99340	1.907E-04	5.208E-04
Test 2	*a*	*0.346*	*0.350*	*7.345E-07*	*1.662E-04*	*0.483*	*0.99677*	*5.195E-06*	*1.119E-04*
	b	0.349	0.355	7.345E-07	2.374E-04	0.690	0.99614	5.489E-06	1.150E-04
	c	0.352	0.360	7.345E-07	3.086E-04	0.897	0.99517	6.39E-06	1.329E-04

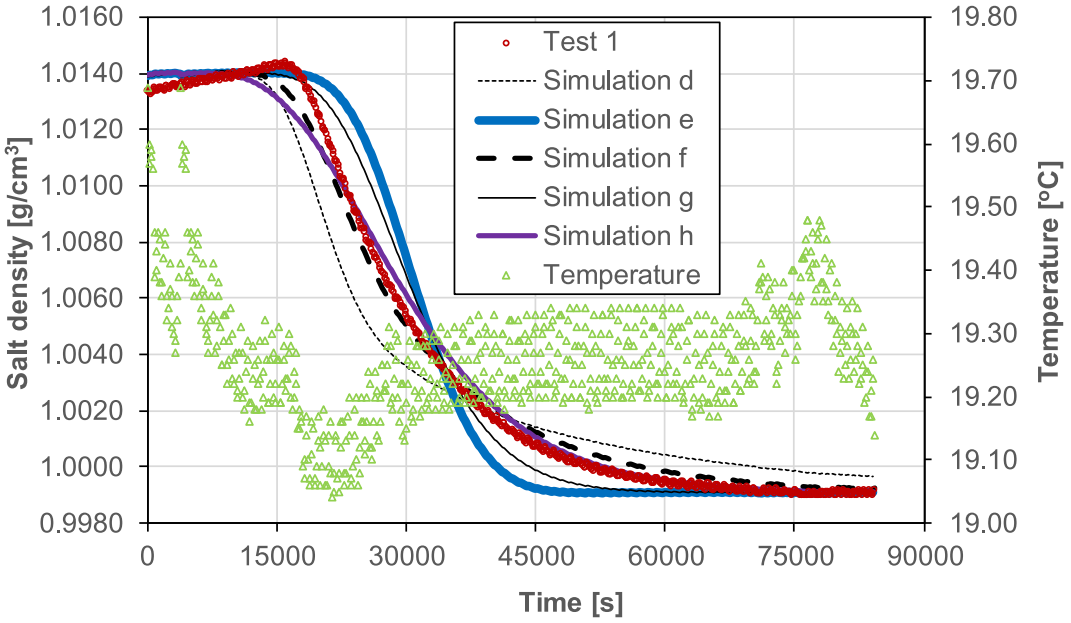

Fig. 8. Breakthrough curves obtained from sensitivity analysis of the salt diffusion coefficient in the clay spheres D_2 (see details for simulation parameters in Table 6) (lines) and the experiment (circles) with the associated temperature data (triangles) for Test 1 (double-porosity medium, saturated case).

not possibly uniform along the soil column. It might be greater at the upper part of medium profile (close to the outlet column). The estimation of the initial concentration for Test 2 (0.9 g/l, Table 1) was not totally satisfactory to simulating this behavior, but globally acceptable to fit the coefficient dispersion.

The dispersivity $\lambda_{DP} = 0.483$ cm was determined from $D_{DP} = 1.662 \times 10^{-4}$ cm^2/s, corresponding to the best fit with the experimental BTC of Test 2 (stepwise test) in the analyzed range of θ_1 and D_{DP}, (Fig. 9, Table 6). This dispersivity was used in direct numerical simulations for other tests: Test 3 (different macroscopic length), Test 7 (different velocity), Tests 5 and 6 (different initial and boundary conditions – pulsewise test). The Péclet number and all statistical indicators were listed in Table 7 for all tests. For the same Darcy velocity, the greater value of *Pe* for the double-porosity medium vs for the single-porosity medium corresponds to a greater D_{DP} vs D_{SP}. It is observed that the numerical simulations reproduced very well the experimental BTCs of the tests (Fig. 10 and 11). For the same Darcy velocity and saturation, the breakthrough time, $t \sim 30000$ s, was longer in Tests 2 (Fig. 9) and 5 (Fig. 11 a) than in Tests 3 (Fig. 10 a) and 6 (Fig. 11 b) where $t \sim 18000$ s. If we refer the saturated case (Test 1) and unsaturated cases (Tests 2, 3, 5, 6 and 7) to the total and effective porosity, respectively, contrary to the single-porosity medium (Tests 8 – 10), the dispersivity is smaller when transport takes place in the total porosity of the sample compared to the case where only a part of the porosity (effective porosity) is explored by the salt solution for the double-porosity medium due to the presence of heterogeneity. To our best knowledge, for the first time, there exists a unique dispersivity value at a given saturation which validates different scenarios of transport in a double-porosity medium,

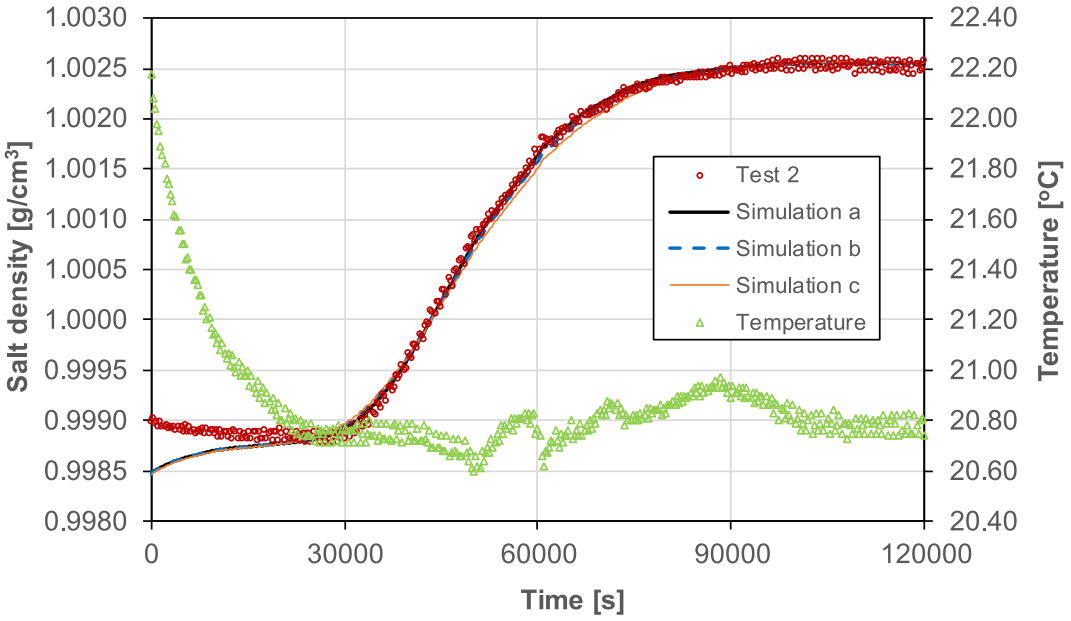

Fig. 9. Breakthrough curves obtained from different simulations (see details for simulation parameters in Table 6) (lines) and the experiment (circles) with the associated temperature data (triangles) for Test 2 (double-porosity medium, case of 86% saturation, fitting stage).

Table 7
Characteristic transport parameters – dispersivity and Péclet number and fitting quality indicators.

Experiment	q [cm/s]	D [cm^2/s]	Pe [-]	λ [cm]	R^2	*SSQ*	*RMSE*
Test 1	5.90E-04	1.899E-04	4.03	0.322	0.99821	5.634E-05	2.831E-04
Test 2	3.44E-04	1.662E-04	2.68	0.483	0.99677	5.195E-06	1.119E-04
Test 3	3.44E-04	1.662E-04	2.68	0.483	0.99816	2.459E-06	7.698E-05
Test 4	3.44E-04	2.713E-04	1.64	0.789	0.99886	1.479E-06	5.956E-05
Test 5	3.44E-04	1.662E-04	2.68	0.483	0.96512	6.677E-07	4.203E-05
Test 6	3.44E-04	1.662E-04	2.68	0.483	0.84531	2.402E-06	6.597E-05
Test 7	5.90E-04	2.850E-04	2.68	0.483	0.99878	5.777E-07	3.223E-05
Test 8	5.90E-04	1.310E-04	1.54	0.089	0.99925	2.227E-05	2.481E-04
Test 9	3.44E-04	4.044E-05	0.97	0.044	0.99049	9.377E-06	1.361E-04
Test 10	3.44E-04	3.839E-05	0.98	0.041	0.99545	5.148E-06	1.055E-04

(Péclet number Pe is calculated by $Pe = \frac{vd_{50}}{D_e}$ for the single-porosity medium and $Pe = \frac{\left(\frac{q}{w_1}\right)\ell}{D_{DP/w1}}$ for the double-porosity medium, where $v = q/\theta$; $d_{50} = 0.0162$ cm; $D_e = 1.545 \times 10^{-5}$ cm^2/s (effective diffusion coefficient of NaCl); $\ell = 1.3$ cm is the characteristic length of the periodic cell of the double-porosity medium).

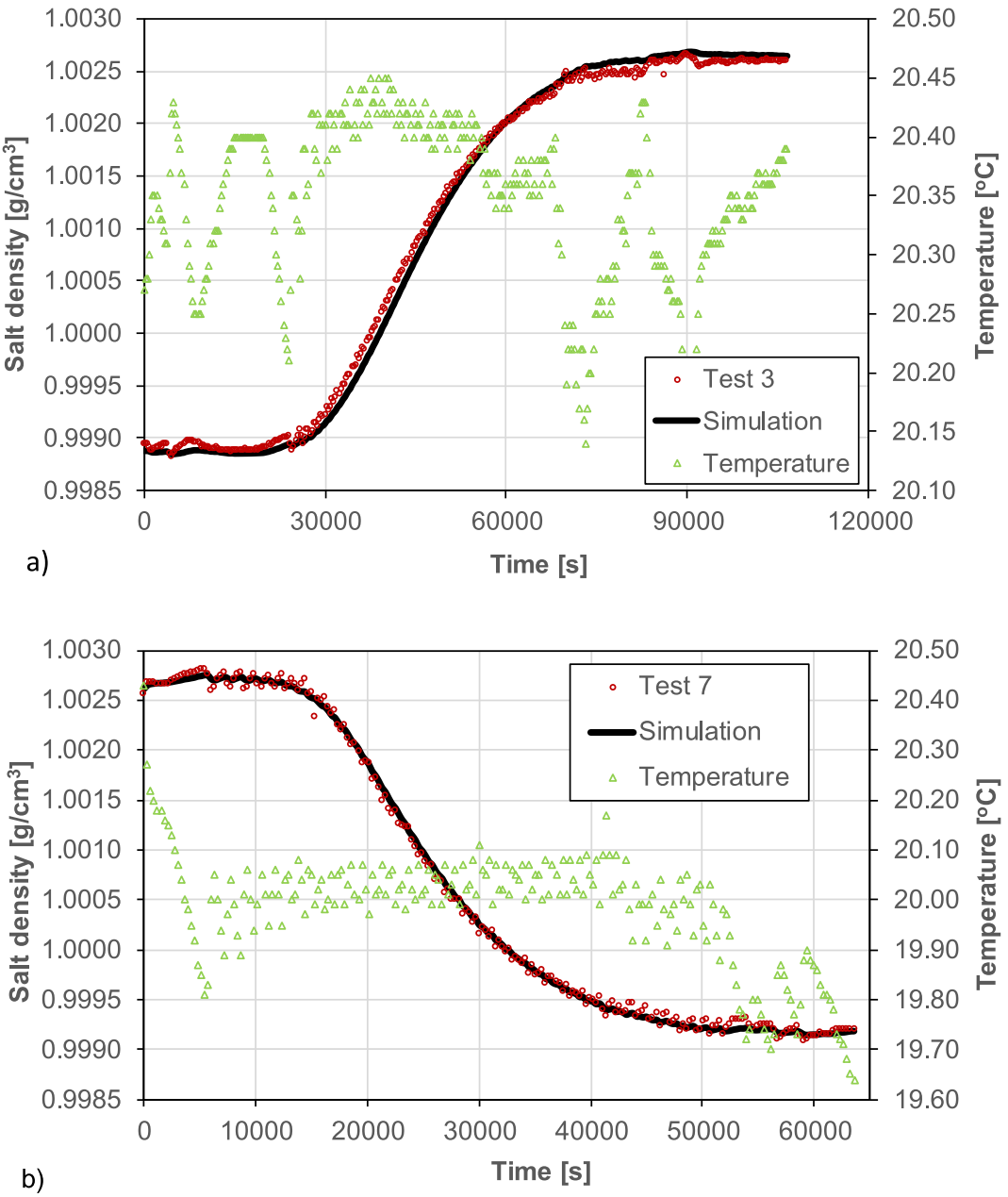

Fig. 10. Breakthrough curves obtained from the simulation (bold line) and the experiment (circles) with the associated temperature data (triangles) for Test 3 (a) and Test 7 (b) (double-porosity medium, case of 86% saturation, validating stage).

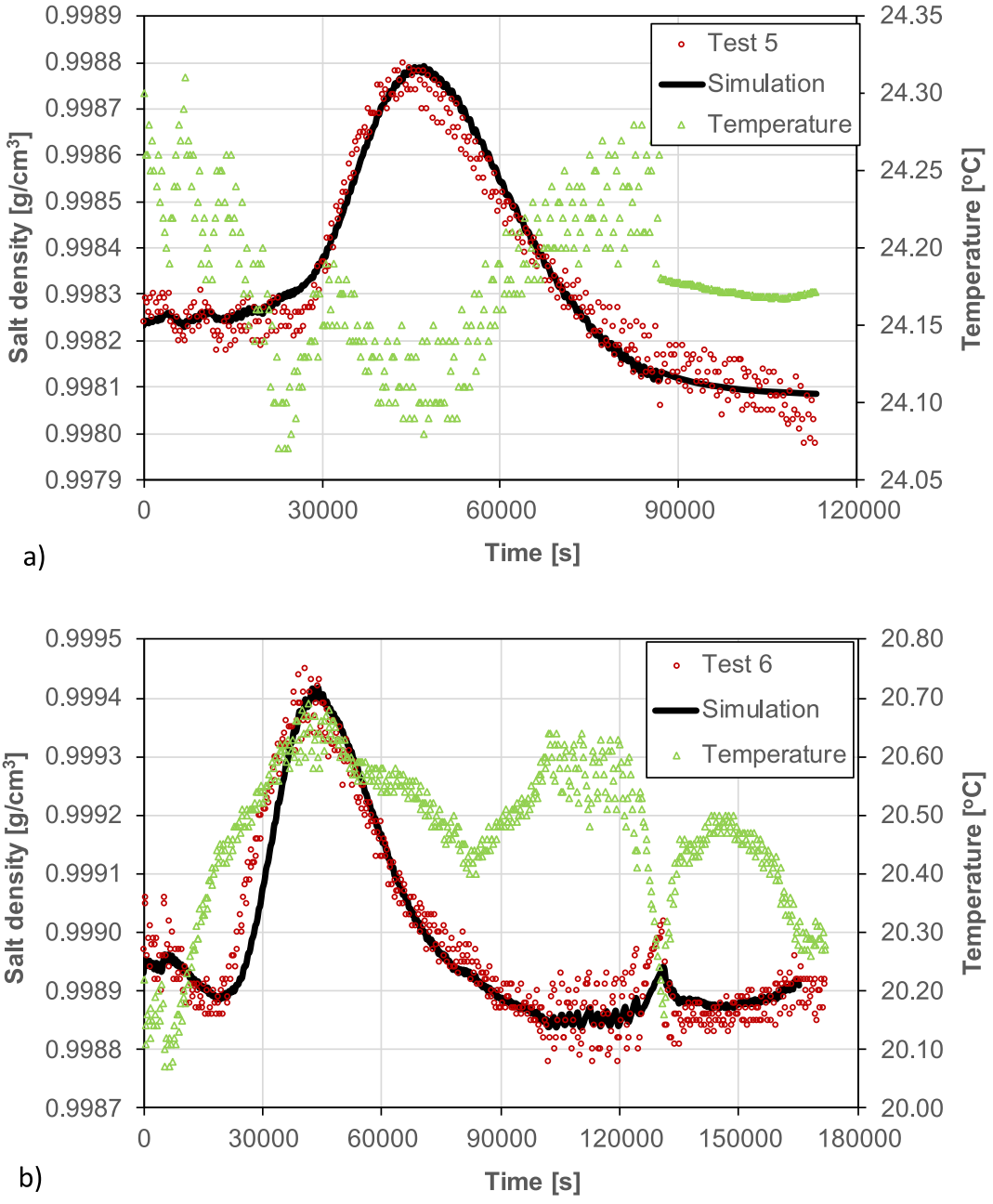

Fig. 11. Breakthrough curves obtained from the simulation (bold line) and the experiment (circles) with the associated temperature data (triangles) for Test 5 (a) and Test 6 (b) (double-porosity medium, case of 86% saturation, validating stage).

regardless of flow and transport conditions.

Fig. 12 displays the very good agreement obtained between the experimental BTC of Test 4 and those obtained by numerical simulation at S_w = 82% using the fitted D_{DP} = 2.713 × 10^{-4} cm^2/s. The dispersivity obtained is 0.79 cm for this case. Consequently, the variation of dispersivity versus saturation could be established for the double-porosity medium in Fig. 13. This relation can be fitted by the power law: $\lambda_{DP} = 0.315 S_w^{-4.5}$ (Fig. 13) that was proposed for single-porosity soils (Nützmann et al., 2002; Toride et al., 2003; Latrille, 2013). Although our experiments concern a limited range of saturation produced by our experimental setup, it can be seen that the dispersivity in the double-porosity medium increases with the diminution of the saturation in the range of this study. This could be explained by the fact that the solute mixing length is much greater not only due to the heterogeneity of the medium (here clay spheres), but also as a result of some disconnections of fluid phases in the medium related to the unsaturated condition of the sample. This trend is in agreement with the findings of previous works in the literature for single-porosity soils (Padilla et al., 1999; Nutzmann et al., 2002; Toride et al., 2003; Sato et al., 2003; Latrille, 2013, among others). For saturation values close to the saturated condition, the dispersivity is of the same order of magnitude as the heterogeneity size in the double-porosity medium (diameter of the clay inclusion), whereas it is of the same order of magnitude as the grain size in the single-porosity medium (Ujfaludi and Maginecz, 1989; Haga et al., 1999; Illangasekare et al., 2010). In the saturation range of 80% – 100%, the dispersivity in the double-porosity medium increases more than the one in the single-porosity soils reported in the literature with an average grain size of 0.20 – 0.28 mm which is of the same order of magnitude as grain size of the sand constituent in the double-porosity medium (0.16 mm) (Fig. 13). The explanation can rely on the increase of tortuosity, in addition to the structural heterogeneity brought by the spherical inclusions.

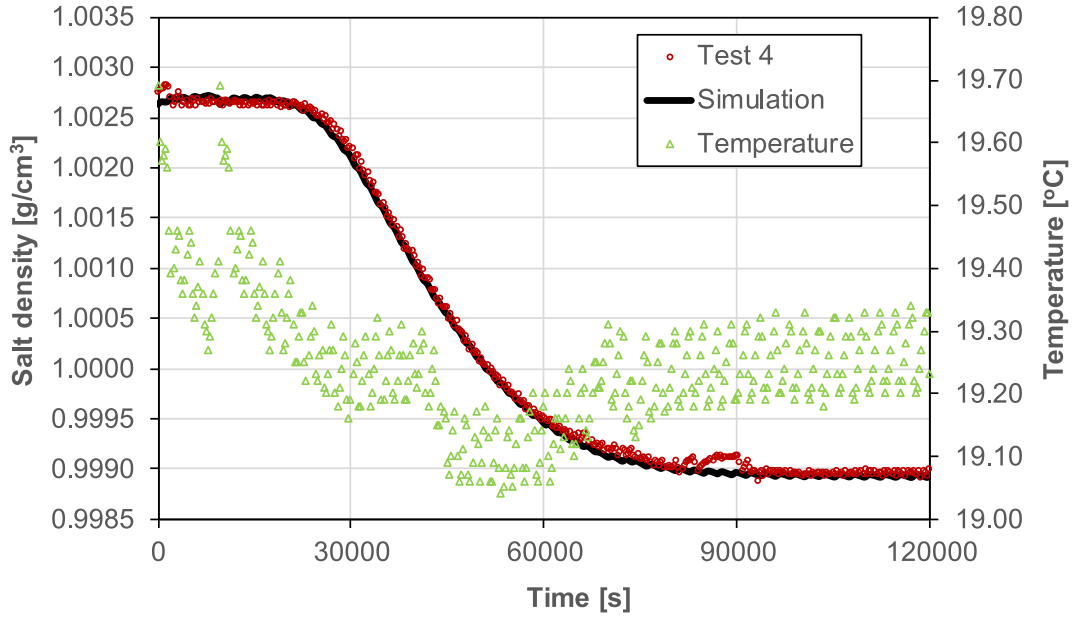

Fig. 12. Breakthrough curves obtained from the simulation (bold line) and the experiment (circles) with the associated temperature data (triangles) for Test 4 (double-porosity medium, case of 82% saturation).

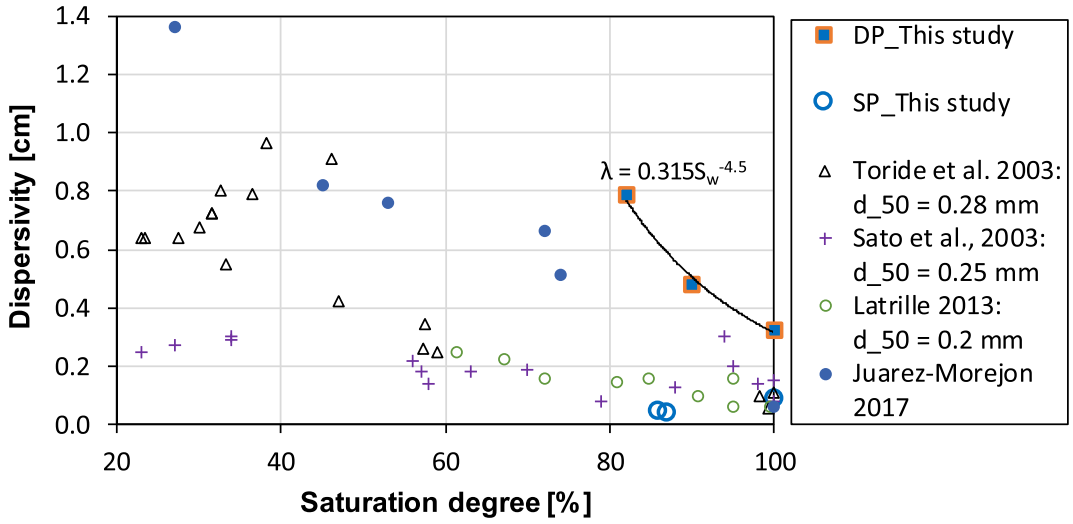

Fig. 13. Dispersivities of the double-porosity medium in function with the saturation obtained in this study, in comparison with the other ones in the single-porosity media available in the literature.

The BTCs obtained for the dispersion tests in the single-porosity medium feature no delay in the solute's breakthrough (Fig. 5 and 6), which can be considered as an indication of the non-existence of dead zones, at least in the sandy matrix, in both types of soil columns. Therefore, the non-Fickian BTCs in the double-porosity medium can be mainly attributed to the presence of heterogeneity, i.e. clay inclusions. The numerical simulations with the obtained dispersivities captured the non-Fickian behaviour of the tracer transport in the double-porosity medium columns. Generally, the agreement between simulated and experimental BTCs is better for the stepwise tests (Tests 3, 4 and 7: Fig. 10 and 12) rather than the pulsewise tests (Tests 5 and 6: Fig. 11). This might be the consequence of the complex non-Fickian mechanism of "tracer flooding water and flooded by water" involved in solute transport during the experiments. In fact, oscillations of density signals in the BTCs of the pulsewise tests were observed. These may be attributed to the switching of the valve twice to change water injection to solute injection and vice-versa, not to mention other accompanying physical mechanisms (temperature variation, ion exchange in the clay, solute washing for the soil column before the tests). For Test 6, the agreement between simulated and experimental BTCs evaluated by R^2 = 0.8453 is not as good as in the other tests. However, the fitting in terms of *SSQ* (2.402×10^{-6}) and *RMSE* (6.597×10^{-5}) is of similar quality as previously presented tests. Note that the number of measured values (*N*) is the greatest in the data of Test 6 with the longest end time of 18×10^4 s (Table 7) and this test has the best mass balance (Table 3). The dispersivity obtained in this study may be considered as a reference value for a medium having a similar REV. It may be also used for a field-scale problem if upscaling conditions are respected, i.e. a REV exists. However, if field-scale permeability is so varied that the local solute dispersion is masked, the value obtained may no longer be applicable.

It must be noted that the BTC data obtained experimentally in this

study may not be convenient for comparison with numerical simulations. Indeed, the successive dispersion tests in the experimental process (although all materials were washed before starting each new test) and the water flow containing other minerals than the used NaCl tracer could have led to modifications of the concentration conditions vs targeted concentrations. The use of a high precision concentration measurement apparatus such as spectrophotometry or electrical conductivity would have allowed a more accurate analysis of the concentration in the porous samples. Indeed, the intermediary step of initial and boundary conditions' concentration estimation and conversion of BTC in concentration into density could also be the sources of further imprecision. Nevertheless, the simulation results using as input the fitted transport parameters reproduce very well all the BTCs and are consistent with the verified mass balance (Table 3). The obtained dispersivities capturing the Fickian and non-Fickian features of the dispersion tests in the single- and double-porosity medium columns, respectively allow us to believe that inherent errors in the experiments, if occurred, like clay particle dispersion, dispersion segregation of high concentration and density flow are negligible.

5. Conclusions

In this study, the non-Fickian transport observed in 1D dispersion experiments in a physical double-porosity medium was quantified. Dispersivity values were obtained by fitting experimental BTCs with ones obtained through numerical simulations with an appropriate two-equation model. Dispersivities of solute transport experiments in single-porosity medium were also determined in order to compare with the non-Fickian dispersivities of the double-porosity medium. These experiments were carried out under different saturation conditions with the control of the water content profiles measured inside the soil samples by a nondestructive gamma-ray technique. In the interpretation of the BTCs, the saturation profiles, therefore, their uniformity or non-uniformity was taken into account. Within the range of the parameters considered in this work, the intrinsic nature of the dispersivity for a given saturation for solute transport in a heterogeneous medium composed of less permeable inclusions in a more permeable matrix has been demonstrated. The intrinsic value found seems independent of exterior loading (different boundary conditions). For high saturation values, the obtained trend between the dispersivity and the saturation in the double-porosity medium is the same as in single-porosity media presented in the literature. In the meanwhile, it could not be concluded definitely whether the trend obtained for the single-porosity medium is in agreement with the findings of previous works.

The present study contributes to the understanding of non-Fickian dispersion as a function of saturation in model heterogeneous double-porosity media. It could be considered as a helpful guide for modelers for estimating the dispersivity in heterogeneous media with variable saturations. It has been shown that the dispersivity of the single-porosity medium should not be used to replace the dispersivity of the double-porosity medium, even if its mobile zone is constituted from the same material as the single porosity medium. Indeed, although the transport in clay nodules is only dominated by diffusion, the presence of these zones, therefore the heterogeneity of the medium has a great influence on the transport of solutes. Only the saturation-dependence of the dispersivity for the single-porosity medium is similar to that of the double-porosity medium.

It is worthwhile to point out that the obtained findings in this study are limited to high saturation values. Further experiments of tracer dispersion for smaller values of saturation in single- and double-porosity media need to be performed in order to generalize and confirm these findings. The results of these experiments will allow to address the validity of the non-monotonic behaviour of the dispersivity versus saturation for double-porosity porous media in comparison with the trend obtained in single-porosity media.

Declaration of Competing Interest

None

Acknowledgements

This research is funded by Vietnam National Foundation for Science and Technology Development (NAFOSTED) under grant number 107.01-2015.25. Tran Ngoc T. D. could do numerical simulations in the I2M thank to the Invited Professor program funding of Bordeaux – INP for his travel. A thank is also addressed to Simon Vedrine (Grenoble – INP), Megane Vogel (EPFL), Nam H. N. Le and Tam N. T. Tran (HCMUT) for participating in this study in CARE Lab.

References

Ahl, J., 2003. Salt diffusion in brick structures. J. Mater. Sci. 38, 2055–2061. https://doi.org/10.1023/A:1023558026018.

Ahmadi, A., Quintard, M., Whitaker, S., 1998. Transport in chemically and mechanically heterogeneous porous media. V: Two-equation model for solute transport with adsorption. Adv. Water Res. 22, 59–86. https://doi.org/10.1016/j.advwatres.2006.10.004.

Aris, R., 1956. On the dispersion of a solute in a fluid flowing through a tube. Proc. R. Soc. London Ser. A 235, 67–77. https://doi.org/10.1098/rspa.1956.0065.

Auriault, J.L., 1991. Heterogeneous medium. Is an equivalent macroscopic description possible? Int. J. Eng. Sci. 29 (7), 785–795. https://doi.org/10.1016/0020-7225(91)90001-J.

Barenblatt, G., Zheltov, I., Kochina, I., 1960. Basic concepts in the theory of seepage of homogeneous liquids in the fissured rocks. J. Appl. Math. 24 (5), 1286–1303. https://doi.org/10.1016/0021-8928(60)90107-6.

Bear, J., 1972. Dynamics of Fluids in Porous Media. Elsevier, New York.

Berkowitz, B., Scher, H., Silliman, S.E., 2000. Anomalous transport in laboratory-scale, heterogeneous porous media. Water Resour. Res. 36 (1), 149–158. https://doi.org/10.1029/1999WR900295.

Bromly, M., Hinz, C., 2004. Non-Fickian transport in homogeneous unsaturated repacked sand. Water Resour. Res. 40 (7). https://doi.org/10.1029/2003WR002579.

Cushman, J.H., Tartakovsky, D.M., 2016. The Handbook of Groundwater Engineering, Third ed. CRC Press, Boca Raton, FL, USA.

De Smedt, F., Wauters, F., Sevilla, J., 1986. Study of tracer movement through unsaturated sand. Geoderma. 38 (1-4), 223–236. https://doi.org/10.1016/0016-7061(86)90017-0.

De Witte, R., 2017. Dispersivity-Saturation Relationship for Various Porous Media; Experiments and Modelling. Master Thesis. Utrecht University.

Dupuy, C., Gharzouni, A., Texier-Mandoki, N., Bourbon, X., Rossignol, S., 2018. Thermal resitance of argillite-based alkali-activated materials. Part 1: effect of calcination process and alkali cation. Mater. Chem. Phys. 217, 323–333. https://doi.org/10.1016/j.matchemphys.2018.06.079.

Fetter, C.W., 1999. Contaminant Hydrogeology, Second ed. Prentice Hall, London.

Fofonoff, N.P., Millard Jr., R.C., 1983. Unesco-IES-80 - Algorithms for computation of fundamental properties of seawater (pp. 58). UNESCO, Paris.

Freyberg, D.L., 1986. A natural gradient experiment on solute transport in a sand aquifer: 2. Spatial moments and the advection and dispersion of nonreactive tracers. Water Resour. Res. 22 (13), 2031–2046. https://doi.org/10.1029/WR022i013p02031.

Fried, J.J., 1975. Groundwater Pollution, Developments in Water Science. 4 Elsevier, New York.

Gaudet, J.P., Jegat, H., Vachaud, G., Wierenga, P.J., 1977. Solute transfer with exchange between mobile and stagnant water through unsaturated sand. Soil Sci. Soc. Am. J. 41, 665–671. https://doi.org/10.2136/sssaj1977.03615995004100040009x.

Gelhar, L.W., 1987. Stochastic analysis of solute transport in saturated and unsaturated porous media. In: Bear, J., Corapcioglu, M.Y. (Eds.), Advances in Transport Phenomena in Porous Media. Springer Netherlands, Dordrecht, pp. 657–700.

Gelhar, L.W., Gutjahr, A.L., Naff, R.L., 1979. Stochastic analysis of macrodispersion in a stratified aquifer. Water Resour. Res. 15 (6), 1387–1397. https://doi.org/10.1029/WR015i006p01387.

Gelhar, L.W., Welty, C., Rehfeldt, R.K., 1992. A critical review of data on field-scale dispersion aquifers. Water Resour. Res. 28, 1955–1974. https://doi.org/10.1029/92WR00607.

Gerke, H.H., van Genuchten, M.T., 1993. A dual-porosity model for simulating the preferential movement of water and solutes in structured porous media. Water Resour. Res. 29, 305–319. https://doi.org/10.1029/92WR02339.

Gharbi, D., Bertin, H., Omari, A., 2004. Use of gamma rays attenuation technique to study colloids deposition in porous media. Exp. Fluids. 37 (5), 665–672. https://doi.org/10.1007/s00348-004-0853-8.

Godoy, A.V., Gomez-Hernandez, J., Zuquette, L., 2018. Scale effect on hydraulic conductivity and solute transport: small and large-scale laboratory experiments and field experiments. Eng. Geol. 243. https://doi.org/10.1016/j.enggeo.2018.06.020.

Golfier, F., Quintard, M., Wood, B., 2011. Comparison of theory and experiment for solute transport in weakly heterogeneous bimodal porous media. Adv. Water Resour. 34, 899–914. https://doi.org/10.1016/j.advwatres.2011.04.019.

Haga, D., Niibori, Y., Chida, T., 1999. Hydrodynamic dispersion and mass transfer in

unsaturated flow. Water Resour. Res. 35 (4), 1065–1077. https://doi.org/10.1029/1998WR900111.
Huang, H., Huang, Q., Zhan, H., 2006. Evidence of one dimensional scale-dependent fractional advection-dispersion. J. Contam. Hydrol. 85 (1–2), 53–71. https://doi.org/10.1016/j.jconhyd.2005.12.007.
Illangasekare, T.H., Christophe, C.F., Fucík, R., 2010. Dispersion and mass transfer coefficients in groundwater of near-surface geologic formations. In: Thibodeaux, L., Mackay, D. (Eds.), Handbook of Chemical Mass Transport in the Environment. CRC Press, Boca Raton, FL, USA.
Irwin, N.C., Botz, M.M., Greenkorn, R.A., 1996. Experimental investigation of characteristic length scale in periodic heterogeneous porous media. Transp. Porous Med. 25, 235–246. https://doi.org/10.1007/BF00135858.
Jougnot, D., 2006. Etude expérimentale et numérique de la conductivité non-saturée dans les milieux à double porosité. Master thesis. Université Joseph Fourier, Grenoble, France.
Jougnot, D., Lewandowska, J., Gotteland, P., Revil, A., 2008. Hydraulic conductivity of unsaturated double porosity geomaterials. In: Paper presented at the The 11th Baltic Sea Geotechnical Conference "Geotechnics in maritime engineering", Gdansk, Poland.
Jougnot, D., Revil, A., Leroy, P., 2009. Diffusion of ionic tracers in the Callovo-Oxfordian clay-rock using the Donnan equilibrium model and the formation factor. Geochim. Cosmochim. Acta. 73, 2712–2726. https://doi.org/10.1016/j.gca.2009.01.035.
Juárez-Morejón, J.L., 2017. Récupération assistée du pétrole par injection de polymères hydrosolubles: Nouvelle approche. Ph.D. Thesis. Université de Bordeaux, Bordeaux France.
Karadimitriou, N.K., Joekar-Niasar, V., Babaei, M., Shore, C.A., 2016. Critical role of the immobile zone in non-Fickian two-phase transport: a new paradigm. Environ. Sci. Technol. 50 (8), 4384–4392. https://doi.org/10.1021/acs.est.5b05947.
Karadimitriou, N.K., Joekar-Niasar, V., Godinez Brizuela, O., 2017. Hydro-dynamic solute transport under two-phase flow conditions. Sci. Rep. 7, 6624. https://doi.org/10.1038/s41598-017-06748-1.
Khan, A.U.H., Jury, W.A., 1990. A laboratory study of the dispersion scale effect in column outflow experiments. J. Contam. Hydrol. 5, 119–131. https://doi.org/10.1016/0169-7722(90)90001-W.
Kutílek, M., Nielsen, D.R., 1994. Soil hydrology. Catena Verlag.
Latrille, C., 2013. Effect of water content on dispersion of transferred solute in unsaturated porous media. Procedia Earth Planet. Sci. 7, 463–466. https://doi.org/10.1016/j.proeps.2013.03.007.
Le Calvé, O. 2002 Température et densité (lecalve.univ-tln.fr › océanographie › température et densité) (Accessed 25 July 2017). Retrieved from lecalve.univ-tln.fr › océanographie › température et densité (Producer). (2002, 25 July 2017).
Lewandowska, J., 2004. Milieux poreux hétérogènes: Modélisation des transferts de masse par homogénéisation. Thèse d'habilitation à diriger des recherches. Université Joseph Fourier, Grenoble, France.
Lewandowska, J., Pilawski, M., 2012. Experiments and micromechanical modelling of elastic parameters of a composite geomaterial. Eur. J. Environ. Civ. Eng. 17 (1), 46–63. https://doi.org/10.1080/19648189.2012.667694.
Lewandowska, J., Szymkiewicz, A., Burzynski, K., Vauclin, M., 2004. Modeling of unsaturated water flow in double-porosity soils by the homogenization approach. Adv. Water Res. 27, 283–296. https://doi.org/10.1016/j.advwatres.2003.12.004.
Lewandowska, J., Szymkiewicz, A., Gorczewska, W., Vauclin, M., 2005. Infiltration in a double-porosity medium: experiments and comparison with a theoretical model. Water Resour. Res. 41 (2), 1–14. https://doi.org/10.1029/2004WR003504.
Lewandowska, J., Tran Ngoc, T.D., Vauclin, M., Bertin, H., 2008. Water drainage in double porosity soils: experiments and micro-macro modelling. J. Geotech. Geoenviron. Eng. 134 (2), 231–243. https://doi.org/10.1061/(ASCE)1090-0241(2008)134:2(231).
Majdalani, S., Chazarin, J.P., Carole Delenne, C., Guinot, V., 2015. Solute transport in periodical heterogeneous porous media: Importance of observation scale and experimental sampling. J. Hydrol. 520, 52–60. https://doi.org/10.1016/j.jhydrol.2014.10.065.
Maraqa, M.A., Wallace, R.B., Voice, T.C., 1997. Effects of degree of water saturation on dispersivity and immobile water in sandy soil columns. J. Contam. Hydrol. 25 (3 – 4), 199–218. https://doi.org/10.1016/S0169-7722(96)00032-0.
Matheron, G., De Marsily, G., 1980. Is transport in porous media always diffusive? A counterexample. Water Resour. Res. 16 (5), 901–917. https://doi.org/10.1029/WR016i005p00901.
Millero, F., 2010. History of the Equation of State of Seawater. vol. 23.
Mishra, S., Parker, J.C., 1990. Analysis of solute transport with a hyperbolic scale dependent dispersion model. Hydrol. Process. 4, 45–57. https://doi.org/10.1002/hyp.3360040105.
Nützmann, G., Maciejewski, S., Joswig, K., 2002. Estimation of water saturation dependence of dispersion in unsaturated porous media: Experiments and modelling analysis. Adv. Water Res. 25 (5), 565–576. https://doi.org/10.1016/S0309-1708(02)00018-0.
Pachepsky, Y., Radcliffe, D.E., Selim, H.M., 2003. Scaling Methods in Soil Physics. CRC Press, Boca Raton, FL, USA.
Padilla, I.Y., Yeh, T.C.J., Conklin, M.H., 1999. The effect of water content on solute transport in unsaturated porous media. Water Resour. Res. 35 (11), 3303–3313. https://doi.org/10.1029/1999WR900171.
Paterson, A., D'Onofrio, A., Allain, C., Hulin, J.P., Rosen, M., Gauthier, C., 1996. Tracer dispersion in a polymer solution flowing through a double porosity porous medium. J. Phys. 6, 1639–1654. https://doi.org/10.1051/jp2:1996153.
Peng, Z., Duwig, C., Delmas, P., Gaudet, J.P., Gastelum Strozzi, A., Charrier, P., Denis, H., 2015. Visualization and characterization of heterogeneous water flow in double-porosity media by means of X-ray computed tomography. Transp. Porous Med. 110 (3), 543–564. https://doi.org/10.1007/s11242-015-0572-z.
Raoof, A., Hassanizadeh, S.M., 2013. Saturation-dependent solute dispersivity in porous media: pore-scale processes. Water Resour. Res. 49, 1943–1951. https://doi.org/10.1002/wrcr.20152.
Robert, T., Martel, R., Lefebvre, R., Lauzon, J.-M., Morin, A., 2016. Field tracer test for the design of LNAPL source zone surfactant flushing. Groundw. Monit. Remed. 36 (2), 68–82. https://doi.org/10.1111/gwmr.12164.
Royer, P., Boutin, C., 2012. Time analysis of the three characteristic behaviours of dual-porosity media. I: fluid flow and solute transport. Transp. Porous Med. 95 (3), 603–626. https://doi.org/10.1007/s11242-012-0065-2.
Sato, T., Tanahashi, H., Loáiciga, H.A., 2003. Solute dispersion in a variably saturated sand. Water Resour. Res. 39 (6), 1155–1162. https://doi.org/10.1029/2002WR001649.
Schoen, R., Gaudet, J.P., Elrickb, D.E., 1999. Modelling of solute transport in a large undisturbed lysimeter, during steady-state water flux. J. Hydrol. 215, 82–93. https://doi.org/10.1016/S0022-1694(98)00263-7.
Schwartz, R.C., Juo, A.S.R., McInnes, K.J., 2000. Estimating parameters for a dual porosity model to describe non-equilibrium, reactive transport in a fine-textured soil. J. Hydrol. 229, 149–167. https://doi.org/10.1016/S0022-1694(00)00164-5.
Sharma, P.K., Abgaze, T.A., 2015. Solute transport through porous media using asymptotic dispersivity. Sadhana 40 (Part 5), 1595–1609. https://doi.org/10.1007/s12046-015-0382-6.
Silliman, S.E., Simpson, E.S., 1987. Laboratory evidence of the scale effect in dispersion of solutes in porous media. Water Resour. Res. 23 (8), 1667–1673. https://doi.org/10.1029/WR023i008p01667.
Simhayov, R.B., Weber, T.K.D., Price, J.S., 2018. Saturated and unsaturated salt transport in peat from a constructed fen. Soil. 4 (1), 63–81. https://doi.org/10.5194/soil-4-63-2018.
Šimůnek, J., Šejna, M., Saito, H., Sakai, M., van Genuchten, M.T., 2013. The HYDRUS-1D software package for simulating the movement of water, heat, and multiple solutes in variably saturated media (pp. 340 (version 344.316)): Department of Environmental Sciences, University of California Riverside, Riverside, California, USA.
Singha, K., 2017. A tale of two porosities: Exploring why contaminant transport doesn't always behave the way It should. Paper presented at the GeoOttawa, Ottawa, Canada.
Sternberg, S.P.K., Cushman, J., Greenkorn, R.A., 1996. Laboratory observation of non-local dispersion. Transp. Porous Med. 23, 135–151. https://doi.org/10.1007/BF00178123.
Sudicky, E.A., 1986. A natural gradient experiment on solute transport in a sand aquifer: spatial variability of hydraulic conductivity and its role in the dispersion process. Water Resour. Res. 22 (13), 2069–2082. https://doi.org/10.1029/WR022i013p02069.
Suresh Kumar, G., Sekhar, M., Misra, D., 2006. Time dependent dispersivity behavior of non-reactive solutes in a system of parallel fractures. Hydrol. Earth Syst. Sci. Discuss. 3, 895–923. https://doi.org/10.5194/hessd-3-895-2006.
Szymkiewicz, A., Lewandowska, J., Angulo-Jaramillo, R., Butlanska, J., 2008. Two scale modeling of unsaturated water flow in a double-porosity medium under axi-symmetric conditions. Can. Geotech. J. 45, 238–251. https://doi.org/10.1139/T07-096.
Toride, N., Leij, F.J., van Genuchten, M.T., 1999. The CXTFIT Code for Estimating Transport Parameters from Laboratory or Field Tracer Experiments (Vol. version 2.1, pp. 137 (version 132.131)). CA, USA: Salinity Laboratory Research Report, Salinity: Riverside.
Toride, N., Inoue, M., Jeij, F.J., 2003. Hydrodynamic dispersion in an unsaturated dune sand. Soil Sci. Soc. Am. J. 67, 703–712. https://doi.org/10.2136/sssaj2003.0703.
Torkzaban, S., Hassanizadeh, S.M., Schijven, J.F., van den Berg, H.H.J.L., 2006. Role of air-water interfaces on retention of viruses under unsaturated conditions. Water Resour. Res. 42 (12). https://doi.org/10.1029/2006WR004904.
Tran Ngoc, T.D., 2008. Transport de solutés dans un milieu à double-porosité non saturé. Modélisation par homogénéisation et application. Ph.D. Thesis. Université Joseph Fourier, Grenoble, France.
Tran Ngoc, T.D., Lewandowska, J., Bertin, H., 2007. Etude experimentale d'un milieu double porosité en condition saturé et insaturé. In: Paper presented at the 18 Congres Francais de Mecanique, Grenoble.
Tran Ngoc, T.D., Lewandowska, J., Vauclin, M., Bertin, H., 2011. Two-scale model of solute dispersion in double-porosity unsaturated media: homogenization and experiments. Int. J. Numer. Anal.l Met. Geomech. 35, 1536–1559. https://doi.org/10.1002/nag.967.
Tran Ngoc, T.D., Lewandowska, J., Bertin, H., 2014. Experimental evidence of the double-porosity effects in geomaterials. Acta Geophys. 62 (3), 642–655. https://doi.org/10.2478/s11600-013-0198-x.
Tran Ngoc, T.D., Ahmadi, A., Bertin, H., 2017. What Can be Learnt About Dispersivity from Transport Experiments in Unsaturated Double-Porosity Soils. Paper Presented at the GeoOttawa, Ottawa.
Tran Ngoc, T.D., Le, N.H.N., Tran, T.V., Ahmadi, A., Bertin, H., 2020. Homogenization of solute transport in unsaturated double-porosity media: model and numerical validation. Transp. Porous Med. 132 (1), 53–81. https://doi.org/10.1007/s11242-020-01380-6.
Ujfaludi, L., Maginecz, J., 1989. Determination of Dispersion Coefficients in Soils Using Their Pore Size Distribution. Paper presented at the International Symposium on Contaminant Transport in Groundwaters.

van Genuchten, M.T., Parker, J.C., 1984. Boundary conditions for displacement experiments through short laboratory soil columns 1. Soil Sci. Soc. Am. J. 48 (4), 703–708. https://doi.org/10.2136/sssaj1984.03615995004800040002x.
van Genuchten, M.T., Wierenga, P.J., 1976. Mass transfer studies in sorbing porous media: I. Analytical solutions. Soil Sci. Soc. Am. J. 40, 473–480. https://doi.org/10.2136/sssaj1976.03615995004000040011x.
Vanderborght, J., Vereecken, H., 2007. Review of dispersivities for transport modeling in soils. Vadose Zone J. 6, 29–52. https://doi.org/10.2136/vzj2006.0096.
Vitorge, E., Szenknect, S., Martins, J.M.F., Gaudet, J.P., 2013. Size- and concentration-dependent deposition of fluorescent silica colloids in saturated sand columns: transport experiments and modeling. Environ. Sci. Process. Impacts. 15 (8), 1590–1600. https://doi.org/10.1039/C3EM30860J.
Wheatcraft, S.W., Tyler, S.W., 1988. An explanation of scale-dependent dispersivity in heterogeneous aquifers using concepts of fractal geometry. Water Resour. Res. 24 (4), 566–578. https://doi.org/10.1029/WR024i004p00566.
Yule, D.F., Gardner, W.R., 1978. Longitudinal and transverse dispersion coefficients in unsaturated plainfield sand. Water Resour. Res. 14, 582–588. https://doi.org/10.1029/WR014i004p00582.